Materials Today • Volume xxx, Number xx • xxxx 2020 RESEARCH

ELSEVIER

RESEARCH: Review

Design of multi-scale textured surfaces for unconventional liquid harnessing

Xin Tang [1,2], Ye Tian [3], Xiaowei Tian [1,2], Wei Li [1,2], Xing Han [1,2], Tiantian Kong [4], Liqiu Wang [1,2,*]

[1] Department of Mechanical Engineering, the University of Hong Kong, Hong Kong
[2] HKU-Zhejiang Institute of Research and Innovation (HKU-ZIRI), Hangzhou, Zhejiang, China
[3] Department of Biomedical Informatics, College of Medicine and Biological Information Engineering, Northeastern University, China
[4] Biomedical Engineering, Shenzhen University, China

The ability to manipulate liquids in a loss-free and refined manner has long been anticipated, with applications in fields such as analytical chemistry, medical diagnosis, and droplet-based manufacturing. The challenge derives from the liquid/solid contacts, which incur spontaneous spreading, strong pinning, and substantial retention. The retention-proof interfaces, including superhydrophobic surfaces, lubricant-infused surfaces, and liquid marbles, mitigate these issues by respectively introducing air, lubricant, and particulate layers to isolate liquids from underlying solids. Assisted by these interfaces, contrastive physical/chemical designs and engineering methods are leveraged to unlock unparalleled liquid-control methods that are otherwise inaccessible. In this review, we focus on the application of retention-proof interfaces in three facets of manipulation: the aliquoting, grip, and transport of fluids. We discuss the key features, strategies and implementations, highlighting the fundamental physics and operation principles. For aliquoting, the cooperation between diminutive geometries and interfaces in partition droplets are examined. For the grip, we discuss the impact of micro-/nanotextures on adhesion behavior and highlight the mechanisms of switching the adhesive forces. For the transport, we review various engineering and functionalizing forms through which subtle driving forces are dexterously imposed on mobile droplets. The performance of different techniques is evaluated, and potential directions are proposed.

Keywords: Droplet; Liquid manipulation; Superhydrophobic surface; Slippery lubricant-infused surface; Liquid marble.

Introduction

The skilful manipulation of tools and objects is a critical foundation upon which humans have built an extremely advanced culture. As confirmed by paleoanthropologists, dexterous human hands allowed our ancestors to develop an intelligent brain [1]. After centuries of technological advancements, humans have developed diverse facilities to maneuver targets beyond the capabilities of our hands. For example, heavy machines such as cranes and loaders were invented to transfer bulky cargo. Likewise, as targets drastically decrease in size, handling difficulty also drastically increases. Small targets such as micro-particles, biological cells, and nano-materials ubiquitously appear in chemical and biological fields. Their micro-manipulation is aided by optical tweezers [2–4], magnetic traps [5–7], atomic force microscope (AFM) tips [8], and electrokinetic forces (for example, electrophoresis and dielectrophoresis) [9–12]. Unlike the handling of small solids, the manipulation of a tiny amount of liquid is further complicated by the liquid/solid contact nature. For example, transporting droplets on or releasing them from a solid

* Corresponding author.
E-mail address: Wang, L. (lqwang@hku.hk)

Please cite this article in press as: X. Tang et al., Materials Today, (2020), https://doi.org/10.1016/j.mattod.2020.08.013

requires forces to overcome the surface tension forces [13]. The maneuvered droplets frequently deposit residues onto solids, causing substantial liquid loss and inevitable intersample contamination [14]. Interestingly, some species have evolved notable strategies for repelling liquids. For example, waxed and nano-textured micro-papillae enable lotus leaves to repel fouling water [15–18], an infused liquid layer makes *Nepenthes* plants slippery for prey and immiscible droplets [19,20], and secreted wax powders help aphids transport their excreted honeydew [13,21]. Such natural creations inspire the development of artificially retention-proof technologies which interface and interact with liquids in a non-wetting, non-sticky, and frictionless manner [13,17,19], thereby laying an essential foundation for loss-free droplet manipulations (Fig. 1).

On an ideally homogeneous surface, a sessile droplet has a spherical cap shape. As described in Thomas Young's pioneering work, the force equilibrium at the three-phase contact line (TCL) determines the contact angle between the liquid/vapor interface and the solid; thereby, for a given system, the intrinsic contact angle θ is a unique value (Fig. 2a, Table 1) [22]. On actual surfaces, chemical and physical heterogeneities inevitably occur, causing a larger advancing contact angle θ_a than the receding one θ_r (Fig. 2b) [23]. The deviation from Young's equation, termed the contact angle hysteresis (CAH) $\Delta\theta$, plays an important role in droplet mobility [24–27]. On a smooth but chemically heterogeneous substrate, Cassie considered the apparent contact angle as an average of the characteristic angles of solid constituents beneath the drop (Fig. 2c) [28]. As a result, if a droplet resides on top of a rough but chemically homogeneous solid, the solid's wettability and non-wetting air pockets contribute to the contact angle (Fig. 2d) [29]. Unlike the Cassie–Baxter state, if the droplet wets and conforms to the topographies of the surface, the apparent contact angle relates to surface roughness as depicted by Wenzel's equation (Fig. 2e) [30,31].

By properly integrating micro-/nano-textures with hydrophobic chemistry, a surface can be made superhydrophobic (SH) (Fig. 2f) [32–34]. On superhydrophobic surfaces (SHSs), the Cassie–Baxter-stated droplet has a high contact angle ($\geqslant$150°) and low CAH, implying limited wettability and enhanced mobility [35]. By impregnating an immiscible lubricant within a functionalized porous substrate, slippery lubricant-infused porous surfaces (SLIPSs) can be fabricated (Fig. 2g) [19,36]. On ideal SLIPSs, a thin lubricant intercalates between the droplet and the solid, removing direct contacts and preserving the droplet integrity [37,38]. The SLIPSs exhibit the ability to repel a wide range of liquids [19]. Another way to prevent wetting is to modify the droplets rather than engineering the substrates (Fig. 2h). By rolling small amount of water (~1–10 μl) over hydrophobic powders, a particle shell is packed on the droplet surface, forming a liquid marble (LM) [13,39–41]. The encapsulating particle layer separates the inner liquid from the substrate, rendering the droplet nonwettable on substrates, including hydrophilic types and liquid baths.

SHSs, SLIPSs, and LMs are topics of great interests as they present many potential applications in areas such as self-cleaning [42–45], anti-fouling [46–49], and fluid drag reduction [50–52]. However, their non-sticky features towards liquids are insufficient to ensure reliable droplet control. To satisfy various facets of droplet manoeuvring, we should be able to precisely aliquot droplets in controlled volumes, reliably transfer droplets among different surfaces, and efficiently transport droplets on a planar substrate. These three aspects of manipulation are relevant to the entire droplet lifetime, from generation to delivery and, finally, removal, and thereby are the focus of this review.

Unlike continuous micro-scale flow, discrete droplets with volumes from the microlitre to the picolitre scale can serve as isolated vessels, precisely metering payloads such as chemical reagents, biological compounds, microorganisms and even fundamental particles [53–56]. The individually addressable sample vessels miniaturize a wide variety of processes, resulting in benefits such as reduced sample consumption [57,58], fast heat transfer [59,60], and well-controlled reaction conditions [61]. As a result, tiny droplets actively participate in various applications such as micro-reactors/-assays, high-throughput screening, and in vitro diagnosis, delivering and transferring materials/energies. Compared with closed-channel-based microfluidics, the droplet-based open system circumvents the clogging problem associated with complex channel networks and has a very straightforward control mechanism without the collaborative work of auxiliary facilities such as pumps and valves [62]. The high flexibility, accessibility, and reconfigurability of droplets on open surfaces also facilitate the integration of different detection or analysis systems [63,64]. By eliminating the liquid retention on surfaces, the manipulating tools or platforms can be adapted for repetitive and multistep usage without cycled rinsing, improving both the time and cost efficiency. The three facets of droplet manipulation are fundamental and key steps in numerous fields. Thus, meth-

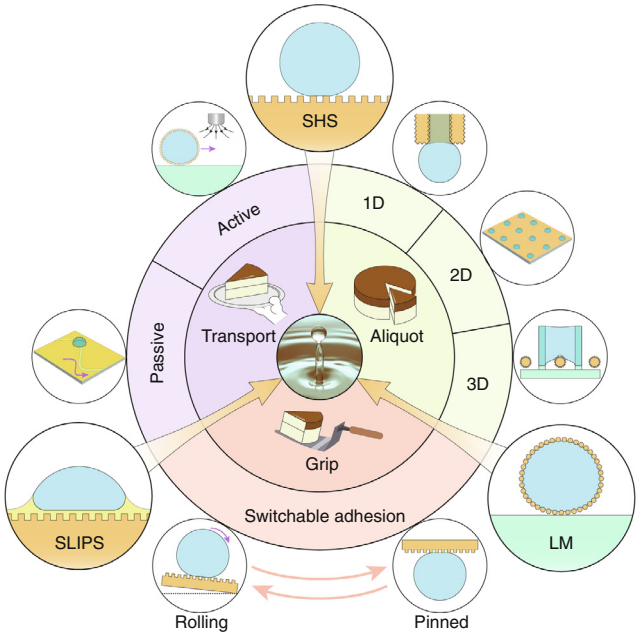

FIGURE 1

Droplets manipulations using retention-proof interfaces. Superhydrophobic surfaces, slippery lubricant-infused surfaces, and liquid marbles aid the aliquot, grip, and transport of tiny droplets, enabling loss-free and effortless liquid manipulation that is otherwise inaccessible. For aliquoting, free tiny droplets can be quasi-statically produced using diminutive 1D, 2D, and 3D geometric configurations. For grip, droplets can be reversibly captured and released in real time. For transport, droplets can be finely navigated in passive as well as active manners.

Please cite this article in press as: X. Tang et al., Materials Today, (2020), https://doi.org/10.1016/j.mattod.2020.08.013

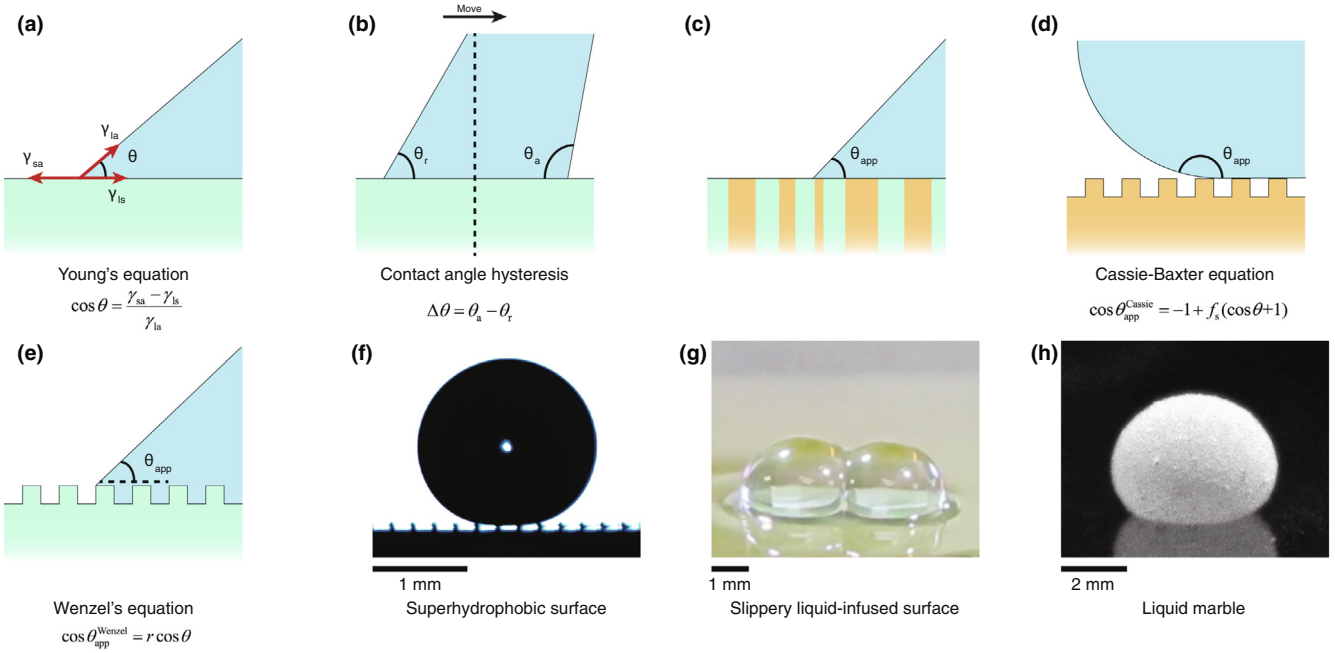

FIGURE 2

Fundamental concepts in liquid/solid interactions and non-wetting interfaces. (a) On a smooth and chemically homogeneous surface, the balance of interfacial forces gives the equilibrium contact angle, and the subscripts s, l, and a denote solid, liquid, and air respectively. (b) For moving contact lines, contact angles deviate from their equilibrium values because of surface heterogeneities. The contact angle hysteresis is defined as the difference between the contact angles at the advancing and receding contact lines. (c) On a smooth but chemically heterogeneous surface, the contact angle is an average of the wettability of each surface constituent. (d) On a textured and chemically homogeneous surface, the contact angle of a Cassie-stated droplet relates to the intrinsic contact angle and solid fraction f_s. (e) The contact angle of a Wenzel-stated droplet relates to the intrinsic contact angle and surface roughness *r*. (f) Integration of hydrophobicity and micro-/nano-scale textures creates SHSs. (g) By infusing an additional immiscible lubricant, the SLIPSs repel a wide range of liquids. (h) Encasing droplets with hydrophobic powders creates non-wetting LMs. Panel (f) is reprinted with permission from Ref. [33], American Chemical Society. Panel (g) is reprinted with permission from Ref. [36], United States National Academy of Sciences. Panel (h) is reprinted with permission from Ref. [41], Elsevier.

ods that can accommodate tiny droplets in a manner similar to the handling of solid objects are highly beneficial. We review research efforts towards the loss-free and dexterous manipulation of tiny droplets with a spotlight on retention-proof interfaces.

Quasi-static aliquot

The generation of micro-to-picolitre droplets is the first step towards minimizing conventional bulk-liquid processes, spanning a wide range of scientific fields and industrial productions. Portable tools such as micropipettes are accurate at the microlitre scale but remain incapable in the submicrolitre range. As the droplet size decreases, its surface-area-to-volume ratio inversely increases, demanding a high-level energy supply to counteract the surface tension. Subsequently, techniques, including inkjet printing, focused acoustic ejection, and electrohydrodynamic printing, have been developed by which droplets are generated using the continuous-jet or drop-on-demand mode (Fig. 3a). For continuous jet printing, a jet is ejected out of a nozzle through a pressure pump and acoustically perturbed to control its breakup into droplets. In contrast, for drop-on-demand, pulsed energy prompts the ejection of a short liquid filament, which then evolves into discrete droplets [65]. Despite the high generation frequency, such methods feature intense actuations. For example, in continuous inkjet printing, the minimum jet speeds required are on the order from 1 to 10 m s^{-1} to gain a sufficiently high Weber number, leading to operating pressures ranging from 30 to 300 kPa [66]. Such high speeds also accompany the generated droplets, offsetting the reliable deposition of droplets on substrates such as SHSs and liquid baths.

Unlike the abovementioned commercialized methods, by coupling wetting-proof interfaces with millimeter-to-micrometer geometries, micro-to-picolitre droplets can also be prepared regardless of intense actuations. The 1D channels, 2D patches, and 3D array layouts are leveraged to offer compact tools to partition liquid in a quasi-static manner, similar to the micropipette serving as a workhorse in laboratories. However, such unique droplet preparations have not yet been reviewed.

1D channels. For inviscid liquid, a slow flow through a nozzle forms a slowly growing pendant droplet, where the gravitational force balances the surface tension, which is referred to as the dripping regime (Fig. 3b) [67]. As described by Tate's law, the pendant droplet masses are proportional to the nozzle sizes, especially the outer diameters because of the spreading on partial-wetting sidewalls. To obviate this limitation, Dong et al. fabricated superhydrophobic nozzles with diminutive inner diameters (~10 μm) as shown in Fig. 3c [68,69]. The flow is fed at a rate so slow that the Weber number is We <~10^{-5}, maintaining the droplet formation in the periodic dripping regime [68]. Otherwise, a higher flow rate can transition the process into the dripping faucet regime accompanied by high droplet volume variation [70]. Liquid spreading on exterior sidewalls is prohibited through the non-wetting nature of superhydrophobicity.

Please cite this article in press as: X. Tang et al., Materials Today, (2020), https://doi.org/10.1016/j.mattod.2020.08.013

TABLE 1

Representative examples of switchable liquid/solid adhesions.

Mechanism	Method	Adhesion (μN)		Advantage	Limitation	Reference
		Non-sticky	Adhesive			
Biphilic surface	Responsive molecules	65	85	Stimuli-responsive, can be incorparated into smart materials system	Switch speed is slow and some stimuli are bio-incompatible	[117]
		6	46			[118]
		12	140			[120]
		8.2	76.7			[122]
		16.1	140.7			[123]
	Mechanical regulation	8.9	100.2	Switch is *in situ* and fast	Prone to retain liquid on hydrophilic microstructures	[81]
Cassie/Wenzel transition	Responsive molecules	4.5	69.2	Ready to implement	Adhesion switch is usually *ex situ*	[124]
	Electro-wetting	5.2	130			[136]
	Pressure impaling	13.2	60.9			[137]
	Sagging transition	30	120			[138]
Pinned fraction tuning	Structural expansion	25	70	Switch is in situ	Difficult to implement	[128]
	Pitch increasing	23	106			[130]
	Composite deformation	45	153			[131]
Holding force	Magnetic force	14	52	Switch is straight-forward and *in situ*	Require superparamagnetic particle doping	[141]
	Negative pressure suction	66	179		Undesired high evaporation rate	[142]

The high on-tip apparent contact angle θ_{app} and small inner channel size D markedly reduce vertical capillary adhesion, which counteracts the gravitational force, causing detached droplets with a volume of $\Omega = \pi\gamma D\sin\theta_{app}/\rho g$, where γ, ρ respectively is the surface tension and density of liquid, and g is the gravitational acceleration [68,70,71]. Using the superhydrophobic nozzles of varied inner channel diameters, nanolitre and even subnanolitre droplets can be produced. Similarly, as the nozzles are made to be superoleophobic, organic liquid with a low surface tension (~26 mN m^{-1}) can be similarly aliquoted [70–72].

2D patches. To increase the generation frequency, Ueda et al. patterned superhydrophobic surfaces with hydrophilic micropatches (Fig. 3d and e) [73]. By moving a liquid source across the biphilic surfaces, the receding contact lines retreat on superhydrophobic regions but remain stuck on hydrophilic ones. Forced sweep triggers consecutive pinch-off of capillary bridges atop the hydrophilic patches, giving rise to numerous microdroplets separated by superhydrophobic boundaries. The microdroplets volumes are determined by the patch area, shapes, liquid surface tensions, and touch-off conditions (preloads and sweeping velocities) [73,74]. The 200×200-μm^2 hydrophilic squares can produce 700-pl water droplets array with a high precision of ~2% [73]. The throughput is so high that an array containing 85,000 droplets can be produced in seconds [73]. The biphilic surface strategy has also been adopted for SLIPSs by patterning pre-lubricated substrates with contrasting liquid affinities (Fig. 3f). As the liquid source contacts the patterned SLIPSs, liquid microdroplets are deposited on regions of higher liquid affinity through lubricant dewet [75]. In this way, liquids with an extremely low surface tension, below 18 mN m^{-1}, can be aliquoted [75].

3D arrays. Inspired by some hydrophyte flowers that close their petals to protect their pollens during flooding, Reis et al. designed radially arranged elastic lamella to grab droplets from water surfaces through self-folding (Fig. 4a and b) [76–78]. The elastic bending is counteracted by the hydrostatic force acting on the lamellar surfaces and surface tension acting on the lamellar edges. If vertically-lifting displacement and lamellar sizes are sufficiently large, the hydrostatic forces dominate the loading [76]. In such cases, as the lamellar size is on the order of the elastogravity length $[B/(\rho g)]^{1/4}$, where B is the bending modulus, the liquid can be encapsulated through petal closing [76]. To fulfill these criteria, the length of the lamella is usually on the millimeter scale, resulting in the uptake of droplets in the microlitre range. Similar configurations, such as radially arranged elastic fiber arrays, have also been widely developed, as shown in Fig. 4c [79,80]. The demonstrated smallest uptaking volume by the fibrous system is ~5 μl for fibers with a length of 2–3 mm. Thereby, further investigations remain necessary to explore the possibility of submicro-to-nanolitre aliquoting using such techniques.

By integrating a superhydrophobic mesh with hydrophilic microfibre arrays, Tang et al. designed a dynamic surface, termed the "mechano-regulated surface (MRS)", enabling the dispensa-

Please cite this article in press as: X. Tang et al., Materials Today, (2020), https://doi.org/10.1016/j.mattod.2020.08.013

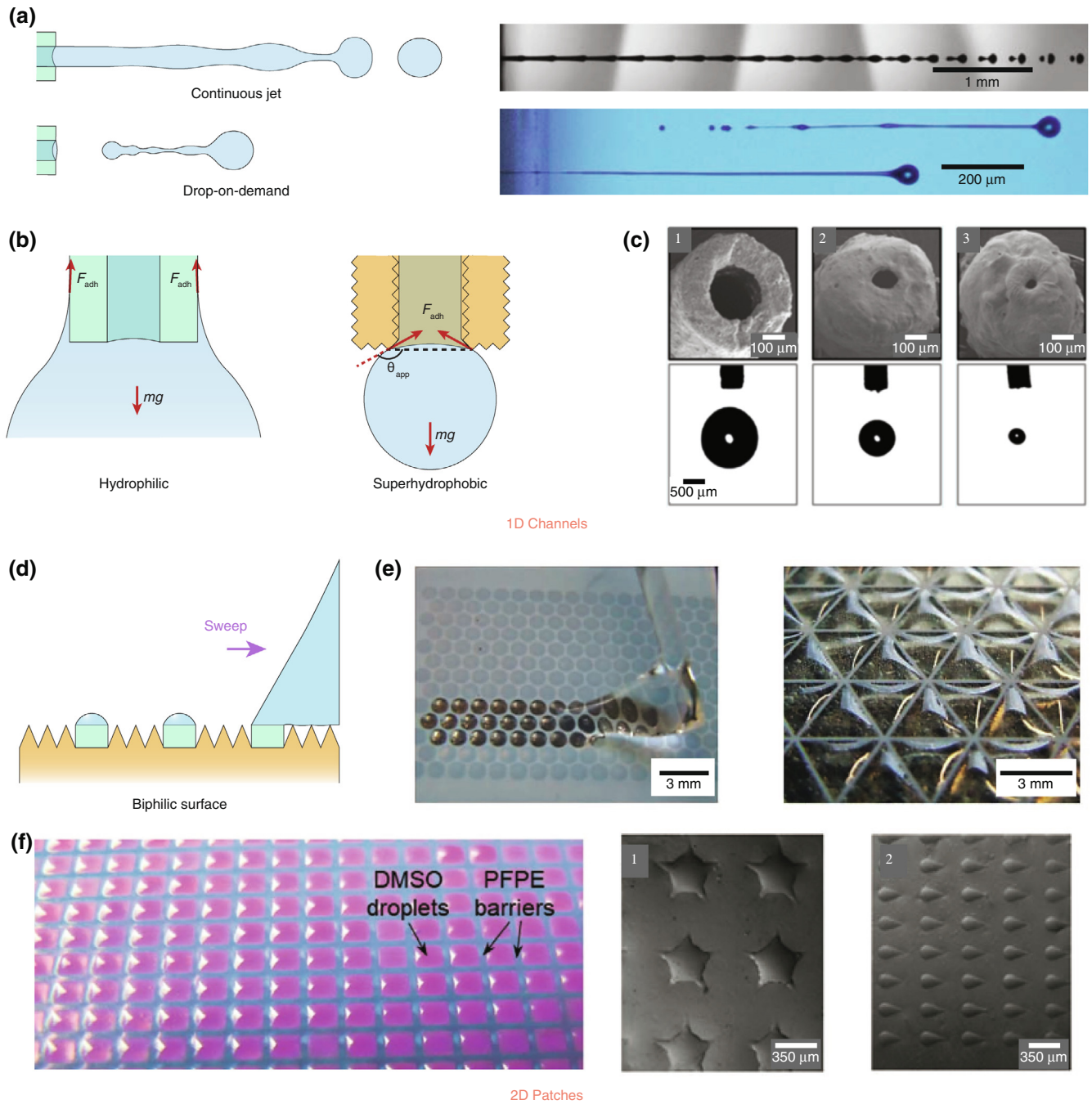

FIGURE 3

Droplet generation through 1D and 2D geometries. (a) High-speed aliquots in the jetting regime. (b) Quasi-static aliquots using superhydrophobic nozzles in the dripping regime. (c) Nanolitre droplets dispensed through superhydrophobic nozzles. (d) The receding TCL is pinned on hydrophilic patches but retreats on superhydrophobic regions, giving rise to partitioned droplet arrays on biphilic surfaces. (e) Water droplet array on biphilic surfaces. (f) Organic liquid droplet array on patterned SLIPSs. The panel in (a) is reprinted with permission from Ref. [65], Wiley-VCH. Panel (c) is reprinted with permission from Ref. [68], American Chemical Society. Panel (e) is reprinted with permission from Ref. [73], Royal Society of Chemistry. Panel (f) is reprinted with permission from Ref. [75], Wiley-VCH.

tion of aliquots onto any type of substrate (Fig. 4d) [81]. Through mechanical reconfiguration, the hydrophilic microfibre arrays can either protrude out of or retract from the non-wetting mesh, causing a reversible switch of the liquid/solid adhesion. As the MRS with a protruded hydrophilic fiber array contacts a liquid reservoir, the fiber array traps a small liquid column among its protruded fibers through liquid wetting, as shown in Fig. 4e. Then, as the hydrophilic fiber array is mechanically withdrawn, the superhydrophobic mesh repels the liquid column, generating a free tiny droplet that can be readily relocated to any targeted place (Fig. 4f). Droplets with a volume ranging from 20 to 200 nl are generated by protruding fibers ranging in length from 100 µm to 1 mm. Thereby, the prepared volume is tuneable, benefiting from the varying microscale features.

Please cite this article in press as: X. Tang et al., Materials Today, (2020), https://doi.org/10.1016/j.mattod.2020.08.013

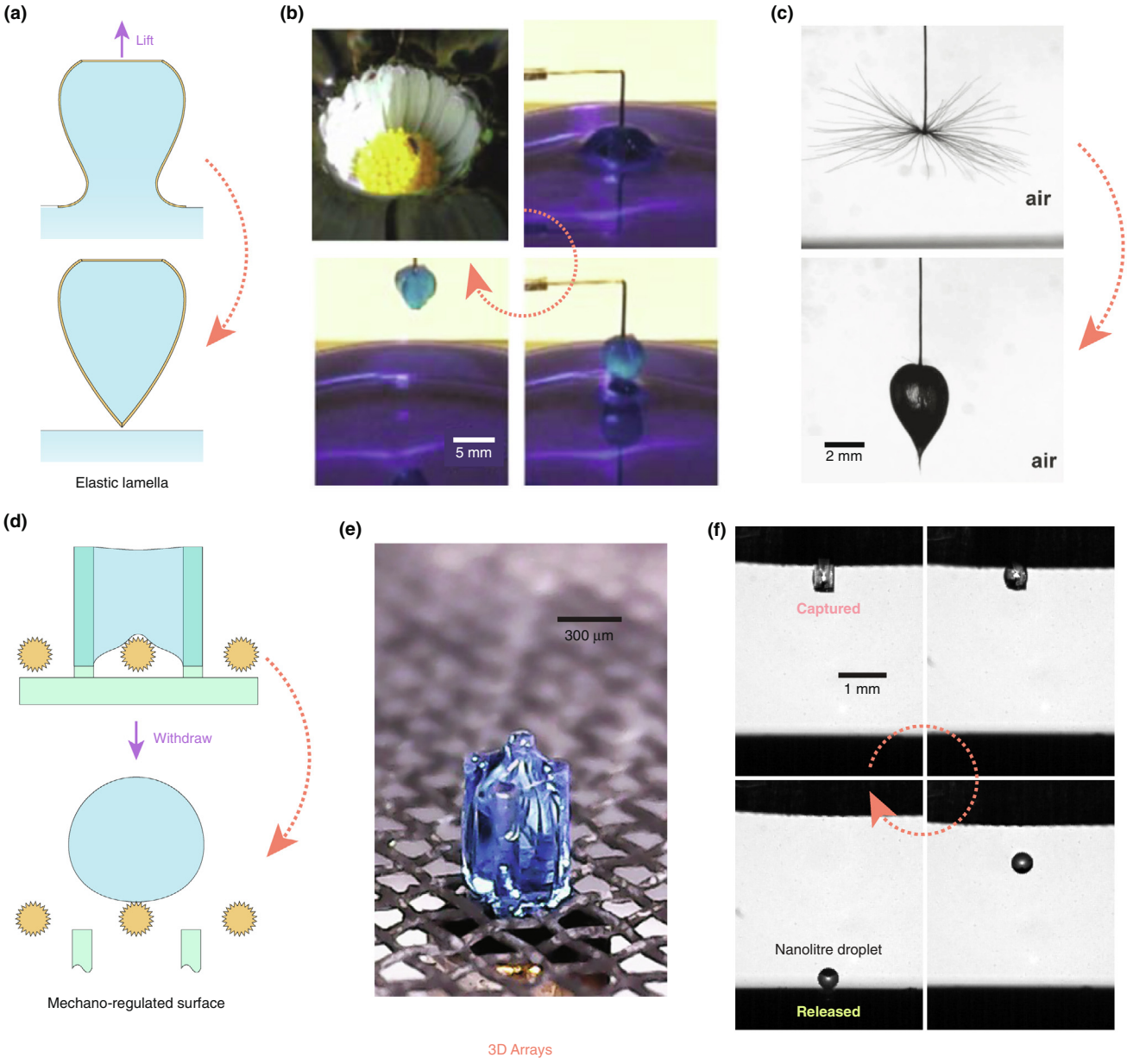

FIGURE 4

Droplet generation through 3D geometries. (a) A radially arranged elastic open system is deformed by touching the liquid reservoir. After it is lifted up, its ends close, containing a liquid portion. (b) The lamella array grabs water. (c) A microfibre array encases a water droplet by closing the ends. (d) A hydrophilic fiber array traps a liquid column by contacting the liquid source. Through fiber withdrawal, the liquid column is repelled by superhydrophobic meshes, generating a free droplet. (e) Trapped liquid column. (f) Generation of a free droplet using the mechano-regulated surface. Panel (b) is reprinted with permission from Ref. [76], Royal Society of Chemistry. Panel (c) is reprinted with permission from Ref. [79], Nature Publishing Group. Panels (e and f) are reprinted with permission from Ref. [81], Nature Publishing Group.

As shown in Fig. 5a, the droplet volume generated by the superhydrophobic 1D channel roughly scales with an inner diameter with a power of 1. On 2D patches, the droplet sizes predictably increase with an increasing patch side length. However, as the geometric sizes of radially arranged elastic "petals" increase, the droplet volume initially increases but eventually plateaus. Thus, the fabrication of those diminutive features is the key to modulate the produced volume. Among the abovementioned methods, 2D patches are usually fabricated through photolithography, which is highly mature and flexible. The characteristic length of the 2D features can vary for 3 orders of magnitude, producing droplets ranging from femtolitres to microlitres. However, the generated droplets are pinned on surfaces, standing in stark contrast to the free droplets produced through 1D superhydrophobic channels and mechano-regulated surfaces. Indeed, the performance of the abovementioned methods still lags behind the conventional techniques, as shown in Fig. 5b. They feature highly simplified and compact designs and a quasi-static partition style. Such mild aliquot styles are preferred in the sorting and isolation of living and fragile

Please cite this article in press as: X. Tang et al., Materials Today, (2020), https://doi.org/10.1016/j.mattod.2020.08.013

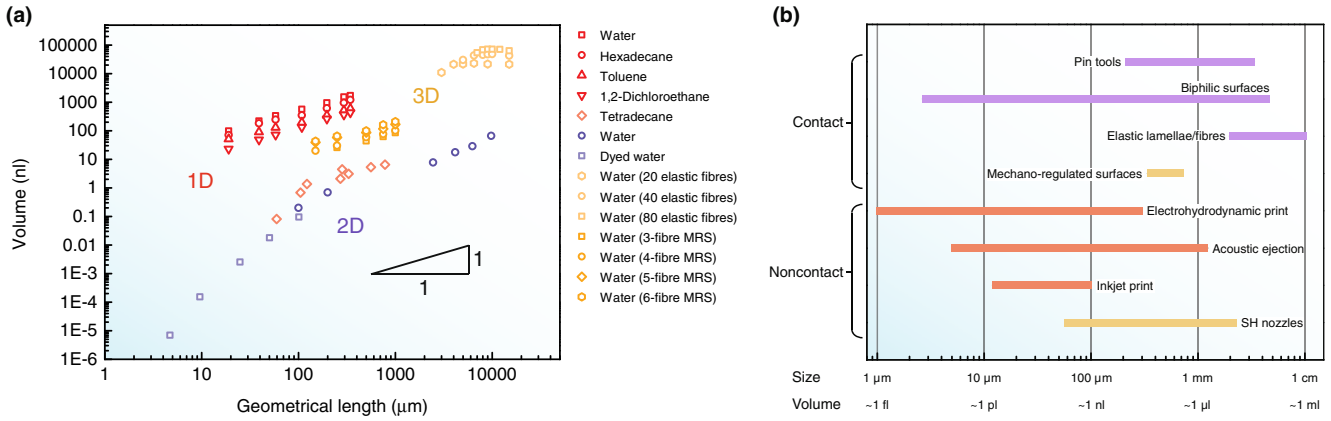

FIGURE 5

Aliquoting performance. (a) The generated droplet volumes strongly depend on the characteristic lengths of the 1D, 2D, and 3D geometries. The characteristic lengths are respectively the inner diameter, side length, and fiber length for the 1D, 2D, and 3D geometries. Data are taken from the literature [70,71,73,74,79,81]. (b) Typical producible droplet volume enabled by different techniques. Purple, red, and orange respectively denote different droplet states that are pinned, freely flying at high speeds, and quasi-statically free. Contact dispense represents methods in which the liquid source has to touch and then withdraw from the substrate to generate droplets through cohesive failures. Noncontact dispense represents methods in which the droplets are ejected out.

matters such as embryos and cells. Further geometric size reduction and parallelization remain necessary to lower the attainable volume and improve production throughput.

Loss-free grip

The generated droplets are frequently gripped to targeted places for further processing. However, when the liquid volumes are small, manipulating tools cannot readily release pinned droplets because of prominent surface tension forces, making the liquid deposition on non-wetting pedestals a difficult task [82–90]. The high adhesion inevitably yields substantial liquid residues on manipulating tools, causing inaccurate transfer and prominent cross-contamination. SHSs with special liquid/solid adhesion have been developed to capture and release droplets. For capture, the surface should be non-wetting but highly adhesive. For release, the surface should be non-sticky to allow free and unbound deposition. Such a dilemma demands a switch in adhesion with maintenance of the overall nonwetting features. Because of great research and industrial interests in such special types of liquid/solid adhesion, numerous works have been reported, and their designs and fabrications have been excellently reviewed by Liu et al. [91,92]. The abundant studies entail diverse materials and chemicals, different physical structures and varying triggering methods, leading to seemingly contrasting mechanisms. Thus, an attempt to comprehensively organize and classify the reported studies on the basis of underlying physics remain necessary.

Liquid/solid adhesion on smooth and structured surfaces. Fundamentally, the interaction at the liquid/solid interface is mainly ascribed to van der Waals forces for organic liquids and additional electrostatic forces for water and ionic solutions [93]. To measure the adhesion between a droplet and a surface, a well-accepted method is to directly pull a contacting droplet off the surface using a precise microbalance. On a smooth surface, the probe droplet successively experiences a snap-in force upon touching, a maximum force during retraction, and a pull-off force upon detachment [94]. Samuel et al. reported that on surfaces of $\theta_r > \sim 90^\circ$, no residue was left behind after the measurement, implying an absolute adhesion failure; otherwise, a supplementary cohesive failure complicates the pull-off force [95]. It is worth noting that the measured forces on structured surfaces depend on the measurement parameters, such as compression distance and probe droplet volume [96,97]. For example, Guo et al. reported that on meshes covered with ZnO nanorods, a compression distance of 20% droplet size can increase the measured adhesion by ~60% [96]. Therefore, standardization of the measurement, including the probe droplet volume, approaching speed, compression distance, and retracting speed, is an urgent need for fair comparisons and evaluations.

Without insights in the intermolecular forces, the thermodynamic work of adhesion relates oppositely to the intrinsic contact angle θ, $W = \gamma(1 + \cos\theta)$ [98]. On smooth surfaces, the water contact angle cannot exceed 120° through known chemical modifications [99]. To inhibit the water attachment, the hydrophobic surfaces are micro-textured to be superhydrophobic. On SHSs, droplets reside on top of the roughness, manifesting the Cassie state [100]. Along the apparent contact line, micro-capillary bridges form at discrete liquid/solid contacts (Fig. 6a and c) [101]. The individual peripheral micro-capillary bridge is similar to a distorted catenoid atop a microscopic asperity (an assumed smooth micropost for instance) and generates a vertical force of $\oint_s \gamma \sin\theta^m ds - \Delta P \times (\pi a^2/4)$, where θ^m is the local contact angle along the post perimeter s, ΔP is the Laplace pressure correlates to droplet radius R as $2\gamma/R$, and a is the post diameter [81]. The Laplace pressure component is usually small compared with the surface tension counterpart, approximating the force to be $\oint_s \gamma \sin\theta^m ds$.

The localized contact angle θ^m along the outer edge of the micropost is smaller than that at the interior edge. As a droplet is lifted from the SHS, micro-capillary bridges immediately stretch, gradually reducing the outermost θ^m. As long as the

Please cite this article in press as: X. Tang et al., Materials Today, (2020), https://doi.org/10.1016/j.mattod.2020.08.013

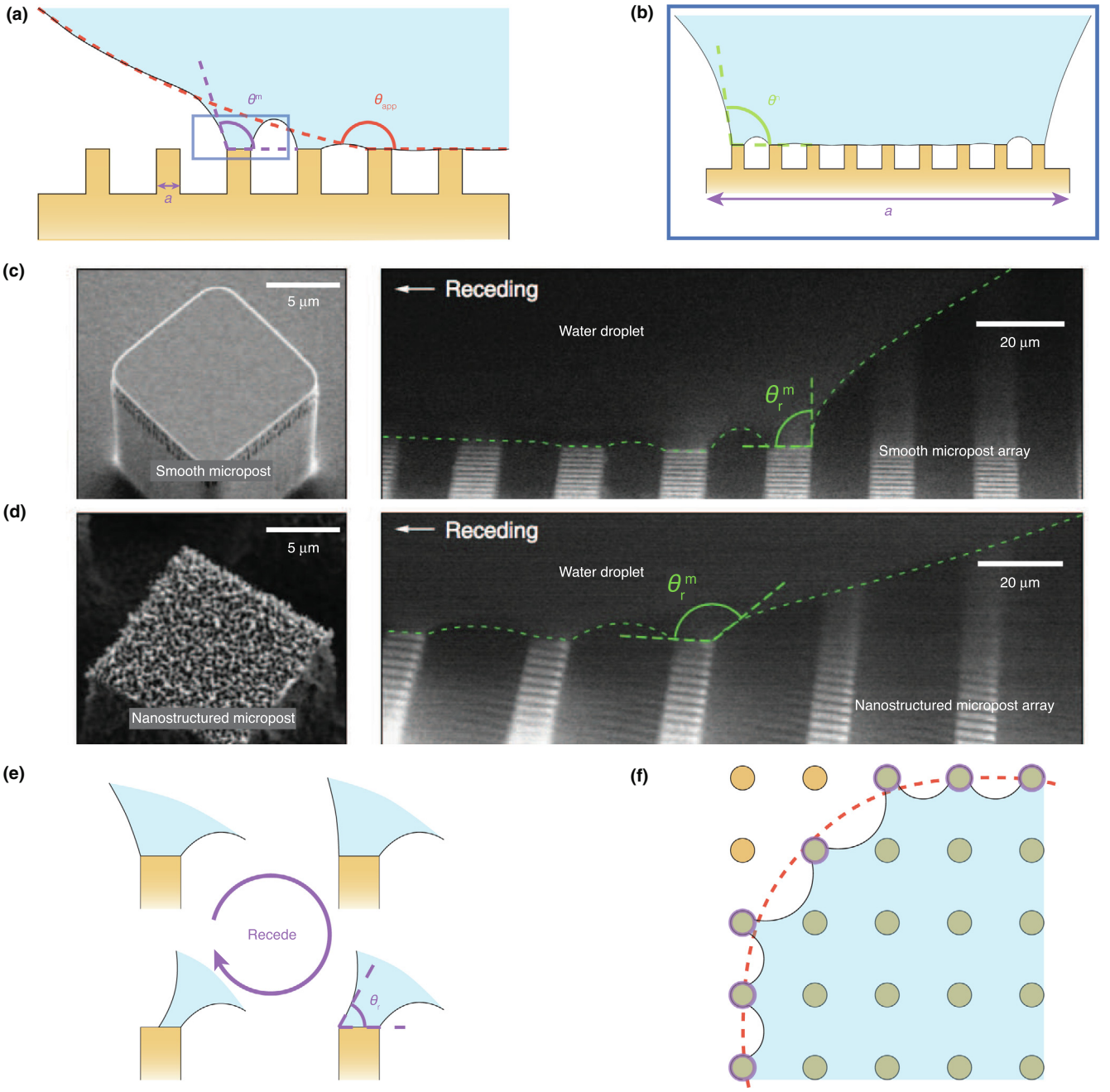

FIGURE 6

Dynamics of micro-capillary bridges. (a) Formation of micro-capillary bridges on microstructured surfaces. Red and purple dashed lines respectively denote the macroscopic and microscopic contact angles. (b) On a nanostructured micropost, the capillary bridges form on the nanoposts in a manner similar to that at the microscale. (c) Scanning electron microscopy (SEM) image of smooth micropost (left) and environmental scanning electron microscopy (ESEM) image of water receding on smooth microposts array (right). Microscale receding contact angle $\theta_r^m \approx 86^\circ$. (d) SEM image of nanostructured micropost (left) and ESEM image of water receding on nanostructured microposts array (right). Microscale receding contact angle $\theta_r^m \approx 140^\circ$. (e) On a micropost, the receding contact line of the capillary bridge is pinned until the microscopic receding contact angle is reached atop the post. (f) Collective pinning of the peripheral capillary bridges. Red dashed line and purple circles respectively denote apparent and actual contact lines. Panels (c and d) are reprinted with permission from Ref. [101], Nature Publishing Group.

microscopic θ^m reaches the intrinsic receding contact angle, the contact line can recede atop the micropost (Fig. 6c–e). Such a receding criterion is validated through direct observation using environmental scanning electron microscopy and laser scanning confocal microscopy [101,102]. Thus, the intrinsic chemistry modulates the microscopic θ^m, which in turn tunes the adhesion. For example, a hydrophilic chemistry tends to pin the contact line even when θ^m reaches 90°, in which case the surface tension contributes entirely to the capillary adhesion.

The overall adhesion is collectively determined by the dynamics of numerous peripheral micro-capillary bridges with sizes and distributions that are delineated by the structural topography. As

Please cite this article in press as: X. Tang et al., Materials Today, (2020), https://doi.org/10.1016/j.mattod.2020.08.013

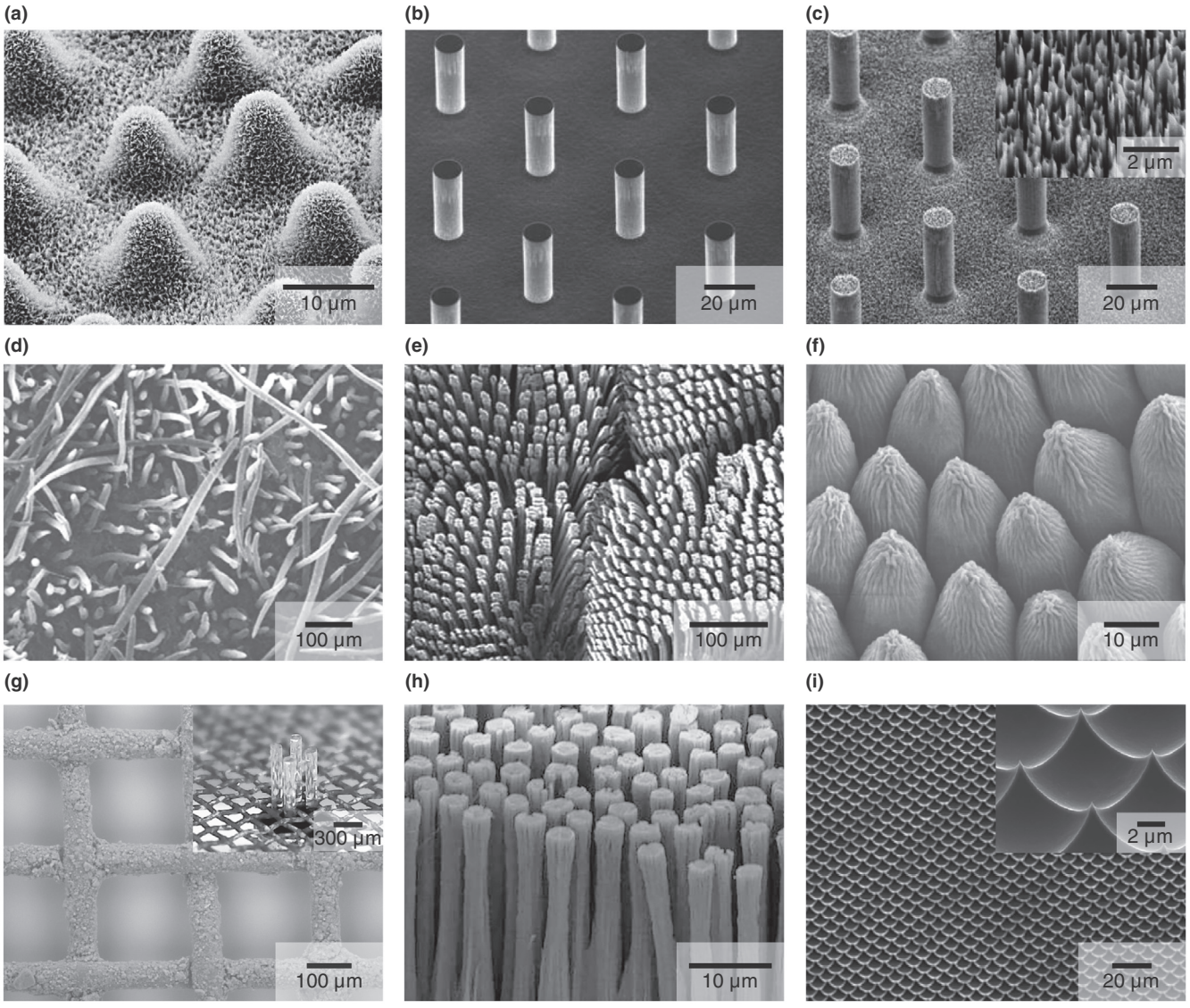

FIGURE 7

Scanning electron microscopy images of representative micro-/nanotextures for superhydrophobic surfaces with different adhesions. (a) Lotus leaves. (b) Microposts. (c) Two-tier hierarchical posts. (d) Peach skins. (e) Gecko feet. (f) Rose petals. (g) Superhydrophobic meshes. The inset is the micrograph of biphilic surfaces consisting of the superhydrophobic mesh and hydrophilic microfibres. (h) Densely packed microposts. (i) Short nanotips. Panel (a) is reprinted with permission from Ref. [18, Beilstein Institute for the Advancement of Chemical Sciences. Panels (b and c) are reprinted with permission from Ref. [34], American Chemical Society. Panel (d) is reprinted with permission from Ref. [111], Elsevier. Panel (e) is reprinted with permission from Ref. [106], Royal Society of Chemistry. Panel (f) is reprinted with permission from Ref. [95], American Chemical Society. Panel (g) is reprinted with permission from Ref. [81], Nature Publishing Group. Panel (h) is reprinted with permission from Ref. [110], Elsevier. Panel (i) is reprinted with permission from Ref. [113], American Chemical Society.

reported by Paxson et al., an effective pinned fraction ϕ is defined as the ratio of the actual peripheral contact line length to the apparent one, ns/l_{app}, where n is the number of peripheral capillary bridges, and l_{app} is the apparent contact line length (Fig. 6f) [101]. On the isotropically arranged micropost array, the pinned fraction ϕ^m is determined by the pitch τ of the microposts as s/τ, making ϕ^m a geometric parameter. By simply assuming that the localized contact angle atop the micropost is an intrinsic receding contact angle θ_r, the vertical adhesion force is simplified as $F/l_{app} = \phi^m\gamma\sin\theta_r$ [101]. If additional nanostructures are overlaid on microposts, the adhesion force on such two-tier hierarchical surfaces becomes $F/l_{app} = \phi^m\phi^n\gamma\sin\theta_r$, where ϕ^n is the pinned fraction on nanostructures (Fig. 6b and d) [101]. For sparsely distributed sharp nanostructures such as nano-grass, the ϕ^n can be as low as ~0.1 [101], allowing highly mobile droplets without a need for microtextures [103]. In contrast, tightly packed nanostructures, including dense nanopillars/nano-tubes inspired by gecko setae reported by Jin et al., can bring about $\phi^n > 1$, where nanostructures counterintuitively enhance the adhesion [104–106]. However, Paxon et al. consider the adhesion enhancing effect of ϕ to saturate when $\phi \geqslant 1.5$ [101]. Such a cut-off is due to the increased interior contact angle caused by the stronger interaction between neighboring capillary bridges on denser structures.

Please cite this article in press as: X. Tang et al., Materials Today, (2020), https://doi.org/10.1016/j.mattod.2020.08.013

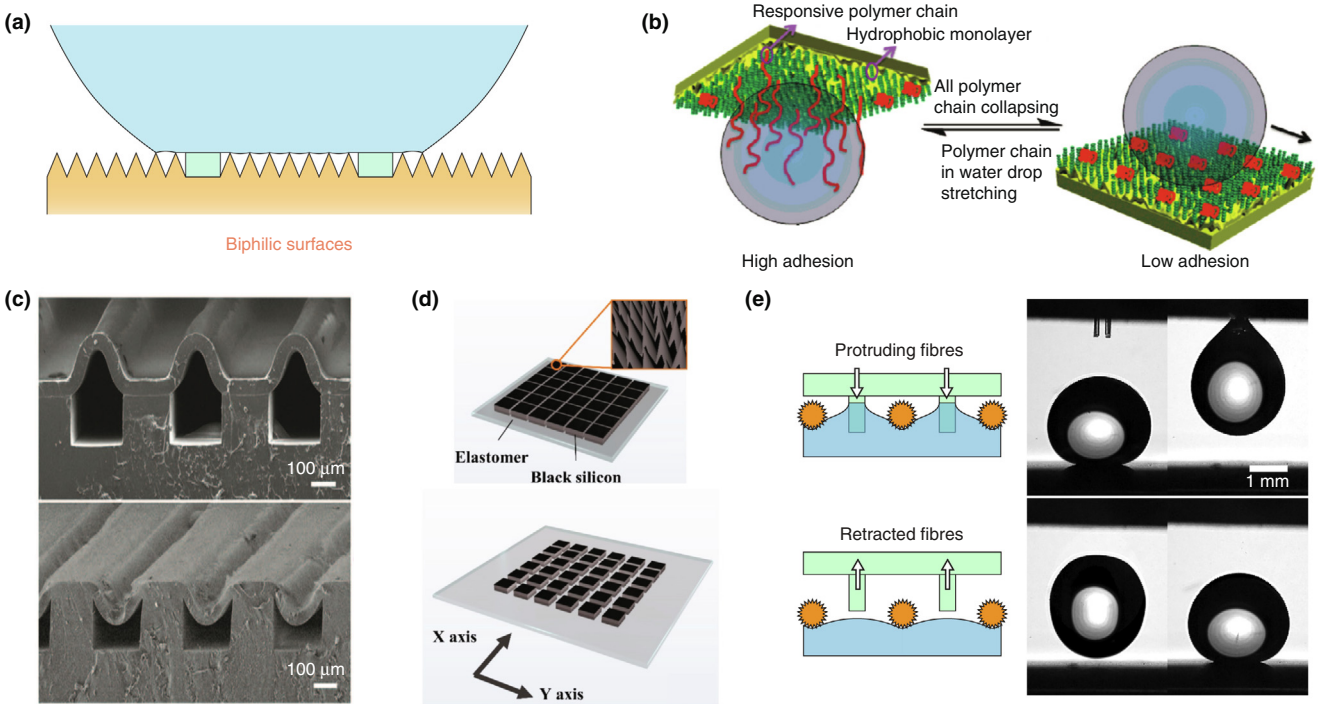

FIGURE 8

Biphilic surfaces to increase adhesive forces. (a) Hydrophilic moieties on a superhydrophobic background provide pinning sites. (b) Adhesion switch on superhydrophobic surfaces decorated with responsive molecules which increase water affinity upon external stimuli. (c) On superhydrophobic background, hydrophilic strips are exposed through inflation and masked through deflation. (d) By stretching the underlying elastomer, the regions of high water-adhesion are exposed; after relaxation, the surface restores its superhydrophobic state. (e) Through protrusion/withdrawal, the hydrophilic fibers are either presented on or hidden behind the superhydrophobic mesh, *in situ* switching the liquid/solid adhesion. Panel (b) is reprinted with permission from Ref. [121], American Chemical Society. Panel (c) is reprinted with permission from Ref. [127], Nature Publishing Group. Panel (d) is reprinted with permission from Ref. [125], American Chemical Society. Panel (e) is reprinted with permission from Ref. [81], Nature Publishing Group.

Adhesive non-wetting surfaces. Apart from reducing intrinsic θ_r and increasing ϕ of Cassie droplets, another approach to improve the adhesion is to switch the droplet states to a Wenzel state. In contrast to the mobile droplets on lotus leaves ($\phi \sim 0.5$) [101], Feng et al. reported that droplets on rose petals experience high adhesion regardless of high contact angles (Fig. 7) [107–109]. The "petal effect" is attributed to the impregnation of water among microstructures, forming a microscale Wenzel state [107]. For Wenzel state droplets, the receding contact line is pinned within rather than atop textures, giving a projected pinned fraction $\phi \geqslant 1$. As a result, the Wenzel state droplets generally adhere on the surface even when the surface is turned upside down.

Petal- and gecko-inspired surfaces have stimulated many works on adhesive SHSs (Fig. 7) [110]. The mechanisms generally fall into the three aforementioned categories and are illustrated in Figs. 8 and 9. To reduce the θ_r, either hydrophilic or hydrophobic patches are sparsely distributed across an SHS, forming biphilic surfaces (Fig. 8). Such biphilic surfaces are presented in natural peach skins, the surface of which is covered by indumentums with contrasting wettability [111]. The background superhydrophobicity preserves the overall non-wetting property, whereas the scattered hydrophilic moieties serve as strong pinning sites. To increase the pinned fraction, topographies such as densely packed post or tubular structures are frequently fabricated. To spontaneously induce the "petal effect", the Cassie-to-Wenzel transition through sag is utilized. As the liquid/vapor interface between structures usually sag with a depth of $\delta \sim \tau^2/R$ (when the structure height is $b < \tau$) [112], to induce the Wenzel state without driving forces, researchers either increase the pitch τ or decrease the height b of the micro-/nanostructures so that $b < \delta$ [113]. As a result, the curved liquid/vapor interface can readily touch the underlying floor, causing liquid impregnation among microscopic structures (Fig. 9a) [114]. Using the above mechanisms, the droplets can be pinned but remain spherical on surfaces.

Switchable adhesion. The post-fabrication adhesion of such so-called adhesive SHSs cannot be modulated due to their fixed microscale structures and chemistries. Thereby, droplets can be captured but remain difficult to release. To tackle such issues, surfaces with reversibly switchable adhesion have been developed (Table 1). Using the biphilic mechanism, SHSs are sparsely grafted with responsive molecules, as shown in Fig. 8b. Once subjected to stimuli, including changes in temperature/pH value, the application of light/electric potential, or presence of ion and solvent [115,116], such responsive molecules can switch their liquid affinity through the rearrangement of molecular conformations [117–119], de-/protonation [120,122], or redox reactions [123,124]. The stimuli-responsive θ_r subsequently brings about changes in adhesive forces. These special chemicals have been reviewed by Fang et al. [116]. However, the response speed is usually slow, requiring minutes to change

Please cite this article in press as: X. Tang et al., Materials Today, (2020), https://doi.org/10.1016/j.mattod.2020.08.013

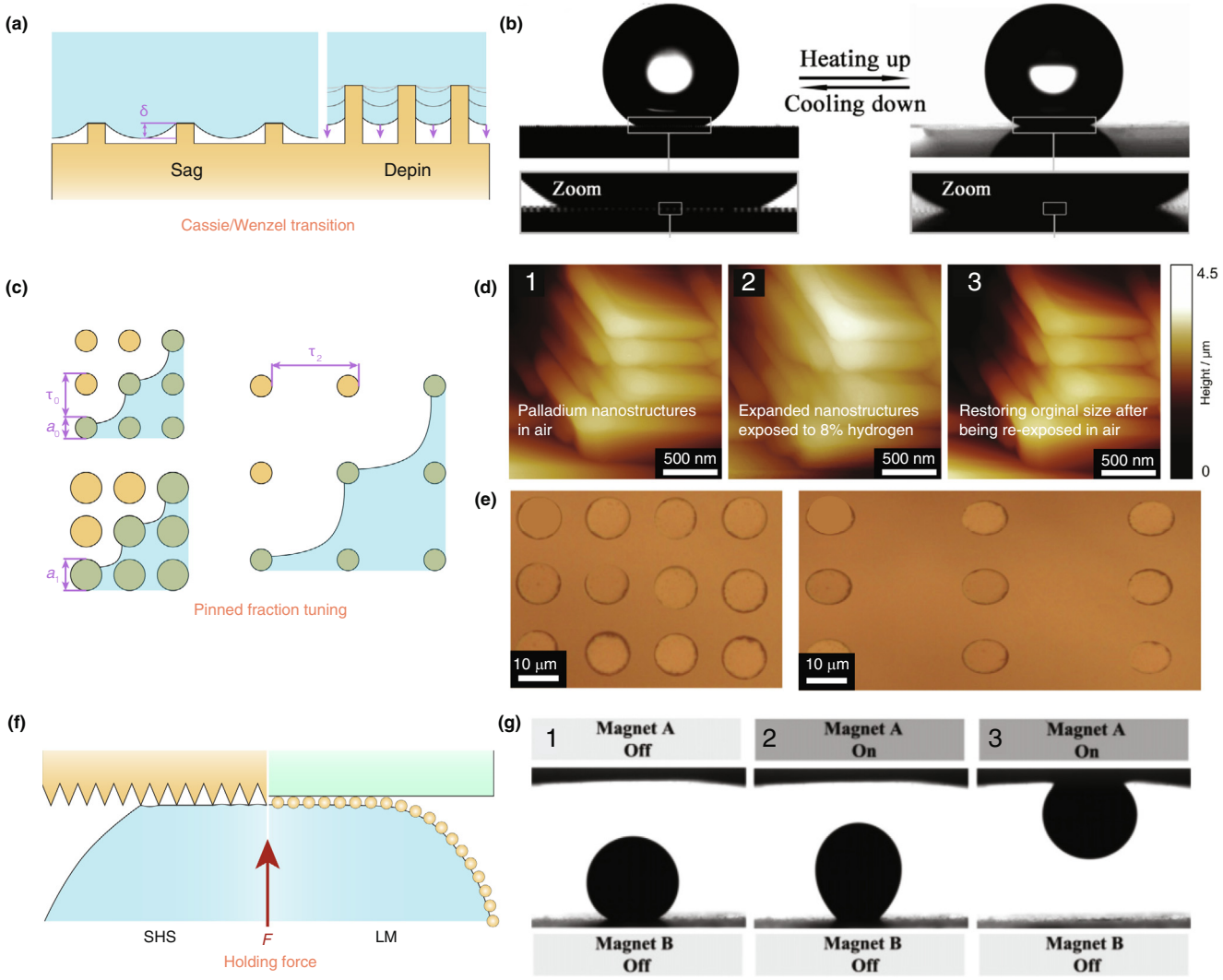

FIGURE 9

Adhesion enhancement on superhydrophobic surfaces of uniform chemistries. (a) Sag of the liquid/air interface or depinning of TCL on vertical walls initiates the Cassie-to-Wenzel transition. (b) Upon heating, grafted responsive molecules switch to be hydrophilic, triggering Cassie-to-Wenzel transition. (c) Structural reshaping, including changes in sizes and pitches, tunes the pinned fraction. (d) AFM images showing the expansion and restoration of palladium structural sizes leveraging hydrogen-driven expansion of palladium; the size expansion increases the adhesion. (e) Increased structural pitch of microposts array through stretch of the elastic substrate. The pitch widening decreases the adhesion. (f) External forces hold droplets on SHSs or capture LMs on surfaces. (g) Droplets doped with magnetic particles are captured on a superhydrophobic ceiling through magnetic forces. Panel (b) is reprinted with permission from Ref. [119], Wiley-VCH. Panel (d) is reprinted with permission from Ref. [128], Wiley-VCH. Panel (e) is reprinted with permission from Ref. [130], Elsevier. Panel (g) is reprinted with permission from Ref. [141, American Chemical Society.

the wettability, which makes real-time switch impossible. Furthermore, some stimuli, including UV light, high voltage, or extreme pH values, are destructive to active biological matters and hazardous to operators, preventing their wide applications.

To obviate the stringent stimuli, dynamic microscopic structures are incorporated to create reconfigurable biphilic surfaces. Those smooth microscopic structures have a higher liquid affinity, and their presence can be regulated through mechanical modulations such as protrusion/retraction [81], stretch/relaxation [125,126], and inflation/deflation (Fig. 8c–e) [127]. Such mechanical reconfiguration proceeds very rapidly, usually in seconds. As the pinning structures present, they locally reduce θ_τ and increase ϕ. Once they are absent on the surface, the superhydrophobicity is restored. However, using such methods, the hydrophilic pinning micro-structures are prone to retaining liquid residues, whereas hydrophobic ones suppress liquid loss but produce an inferior adhesive performance. As a result, a trade-off exists between liquid loss and adhesion.

To exclude the hydrophilic moieties, surface topography is reversibly reshaped to tune the pinned fraction ϕ, which we termed the pinned fraction tuning mechanism (Fig. 9c). Expansion of the structures leads to an increased ϕ and, thereby, enhanced adhesion. Such a switching pathway has been achieved by Seo et al., who exposed palladium-coated silicon nanowires to hydrogen to induce structural volume expansion (Fig. 9d) [128,129]. In contrast, by increasing the structural pitch τ, ϕ decreases, switch-

Please cite this article in press as: X. Tang et al., Materials Today, (2020), https://doi.org/10.1016/j.mattod.2020.08.013

ing the adhesion from high to low. Wang et al. reported that by stretching an elastic film patterned with micro-posts, the pitches are increased by twofold, decreasing the water droplet adhesion from 106 to 23 μN (Fig. 9e) [130]. More commonly, the change in the two parameters are interwoven, resulting in complicated impacts on adhesion. For example, Yang et al. reported that by bending the magnetized micro-needles, more liquid/solid contacts are formed, resulting in high adhesion [131]. However, because of the design and fabrication difficulty, the pinned fraction tuning mechanism is only sporadically reported. The liquid residue and switching speed remain unreported.

Another widely reported mechanism is to transit the droplets between the Wenzel and Cassie states, which we simply termed the Cassie/Wenzel transition mechanism. Li et al. reported a wide thermodynamic map for the wetting states and demonstrated the condition where Cassie is the stable state [132]. However, such cases are rarely encountered because of the strict criterion. For example, for an SHS with a solid fraction f_s of 0.1 and micropost aspect ratio of 2, the intrinsic water contact angle θ has to exceed 122°, surpassing the upper limit of hydrophobic chemistries.

On most surfaces, the Cassie and Wenzel states are respectively metastable and stable states and separated by an energy barrier [133]. Bormashenko has thoroughly reviewed the wetting transitions [133]. Gently deposited droplets remain in the Cassie metastable state [132]. To pin them through a Cassie-to-Wenzel transition, a critical pressure difference across the liquid–vapor interface $\Delta P_c = -s\gamma\cos\theta/(\tau^2 - s^2/4\pi)$ has to be surmounted [133,134]. As ΔP_c is reached, the TCL on the micropost top depins and advances downward, causing collapse of the Cassie state (Fig. 9a). Such a vertical depinning pathway can be facilitated by mildly decreasing the intrinsic contact angle θ (Fig. 9b). By either grafting responsive polymers or utilizing electro-wetting phenomena, the surface's water affinity can be enhanced to induce a Cassie-to-Wenzel transition [119,135,123,124]. An alternative method is much more straightforward, which is to apply external forces, for example magnetic forces, to reach ΔP_c [137]. Apart from the depinning pathway, the aforementioned sagging transition is also utilized to switch the adhesion. Through reversible topographical deformation, the surface roughness can be switched between high and low states, which respectively favor the Cassie and Wenzel states [138,139]. However, the higher energy barrier from the stable Wenzel state towards the metastable Cassie state makes the adhesion switch *ex situ*, which means that after the sticky surface has been changed to be non-adhesive, newly deposited droplets exhibit Cassie states, whereas previously pinned droplets still remain their Wenzel states [91].

The *in situ* switch is critical for droplet grip, otherwise captured droplets cannot be released from the reversible surface. However, such an important property has still not been explicitly reported in some works. Methods exploiting the Cassie/Wenzel transition usually suffer from *ex situ* adhesion switch. Wu et al. reported that by inducing a large substrate curvature, the Wenzel-to-Cassie transition can be achieved by injecting air beneath droplets [140]. By contrast, some techniques adopting the biphilic and pinned fraction tuning mechanisms are shown to enable the *in situ* adhesion switch [81,118,120,121,130,126,127]. Another method that enables an *in situ* switch is to utilize holding forces such as magnetic forces and negative-pressure suction [141,142], to hold droplets on an SHS (Fig. 9f and g). Such methods are very straightforward as the on/off of external forces directly dictate the droplets' pinned/released states. However, external-force-assisted grip is rarely reported, and the existing methods have some limitations, including the need for superparamagnetic particle doping and enhanced evaporation rates. The holding-force strategy is also utilized to handle liquid marbles to circumvent the manual-handling drawbacks, including inconvenience, inconsistency and easy marble breaking [143,144].

In Fig. 10, we provide an overview of the water droplet pull-off forces on different types of surfaces reported in the literature [81,95,105,108,111,117,118,120,128,130,131,140,142,122–124,136–138,145–168]. This is a general comparison owing to the non-standardized measurements. On smooth surfaces, it has been identified that a high receding contact angle generally leads to a reduced pull-off force [95]. By introducing different levels of textures, so-called adhesive SHSs are widely reported and studied. Their adhesive performances widely vary because of the contrasting structures and chemistries they used. Their upper adhesion limit is on par with that of smooth surfaces as the pinned fraction has an upper threshold value. On surfaces with switchable adhesion, their maximum and minimum forces dictate their droplet grip performance. Simply neglecting the change in droplet/-surface contacting perimeters for different droplets volumes, as long as the droplets' gravitational forces fulfill $F_{adh}^{min} < mg < F_{adh}^{max}$, where F_{adh}^{max} and F_{adh}^{min} are respectively the maximum and minimum adhesion, the capture and release can be achieved through the *in situ* switch. However, many works lack the force measurement and only demonstrate the switch

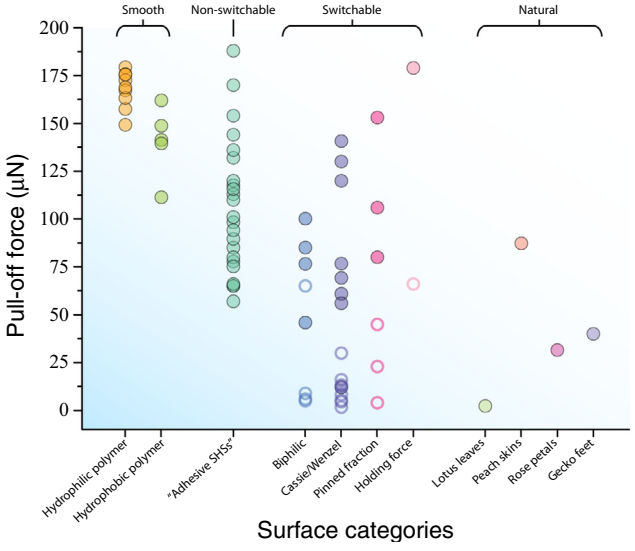

FIGURE 10

Adhesive performances. Pull-off forces for different surface categories. Data are taken from the literature [81,95,105,108,111,117,118,120,128,130,131,140,142,122–124,136–138,145–168]. For switchable surfaces, filled circles denote adhesive states and open circles denote nonsticky states.

Please cite this article in press as: X. Tang et al., Materials Today, (2020), https://doi.org/10.1016/j.mattod.2020.08.013

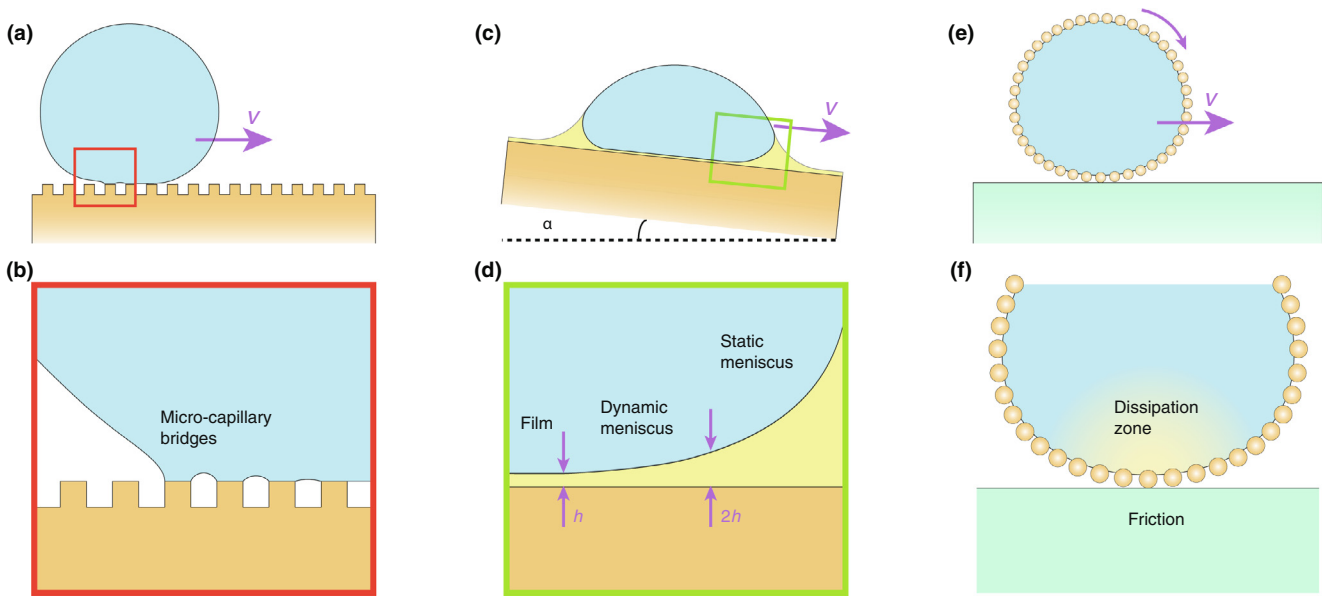

FIGURE 11

Motion resistances associated with retention-proof interfaces. (a) Schematic of a rolling droplet on an SHS. (b) On SHSs, micro-capillary bridges situated at the apparent receding contact line resist the motion. (c) Schematic of a droplet sliding on an SLIPS tilted at an angle of α. (d) On SLIPS, the drag force relates to the Landau–Levich–Derjaguin flow at the front meniscus. (e) Schematic of a rolling LM. (f) The friction and internal viscous dissipation resist the motion.

through mobility change, leading to an insufficient performance characterization. The F_{adh}^{max} for high adhesive states and F_{adh}^{min} for low adhesive states overlaps for different methods; thereby, it would be better if benchmark values for the two states can be determined. Generally, the artificial adhesive surfaces' performances surpass their natural counterparts, including peach skins, rose petals, and gecko feet, which correspond to mechanisms of the biphilic surface, Cassie-to-Wenzel transition, and increased pinned fraction, respectively. For reported switchable surfaces, the average force difference between two extrema is ~76 μN. Thereby, further increasing the F_{adh}^{max} and decreasing the F_{adh}^{min} can widen the transferable droplet volumes. Moreover, as measured pull-off forces relate to the apparent contact line length l_{app} upon detachment, it may be more meaningful if the adhesive performance is characterized by F_{adh}/l_{app} rather than only F_{adh}.

On-plane transport

Being transferred onto the targeted platform, the addressable droplets, acting as samples vessels, are transported across the surface for processes such as reagent delivery, micromixing or sorting [169–172]. Droplet locomotion plays key roles in the precision as well as efficiency of all those processes, which makes the refined navigation, including controls on velocities and directions, become a priority. Retention-proof techniques are utilized to suppress liquid loss and minimize the pinning from underlying substrates, allowing motion initiation upon subtle driving forces [143,173–183]. Thus, the manners in which the delicate driving forces are imposed and wielded directly delineate the flexibility, accuracy, working range of the navigation. Moreover, an understanding of typical motion resistance associated with various retention-proof interfaces is also critical for the on-plane transports.

Characteristic resistance. The droplet mobilities using the retention-proof interfaces are usually characterized through the descending motion on titled substrates. On the basis of droplet temporal displacements, the interfacial interactions are then inferred. As the study advances, cantilever-based force sensing systems are utilized to enable the real-time detection of the subtle resistance, detailing the motion dynamics and deepening understanding on interfacial contacts [184,185]. The resistances associated with SHSs, SLIPSs, and LMs differ from each other (Fig. 11). When a liquid droplet initiates its motion on an SHS, the advancing front of the droplet readily lies on the solid textures ahead, whereas the receding rear is pinned on asperities (Fig. 11a) [186–188]. As a result, the micro-capillary bridges situated at the receding contact line produce resisting forces against the motion (Fig. 11b) [101]. The resistant force F_γ associates with CAH as $F_\gamma = 2w\gamma(\cos\theta_r - \cos\theta_a)$, where w is the droplet/surface contact radius and can be approximated as $w \sim R\sin\theta_{app}$ on SHSs [189–193].

On SLIPSs, the remarkable liquid repellence is due to a nanometre-thick lubricant film intercalating the droplets and underlying solids (Fig. 11c). The film remains intact when the thermodynamic (the spreading coefficient $S = \gamma_{ls} - (\gamma_{lo} + \gamma_{os}) \geqslant 0$, where the subscripts l, o, and s denote liquid, lubricant, and solid respectively) as well as dynamic (Hamaker constant $A > 0$) criteria are both satisfied; otherwise, the liquid partially or even completely displaces the lubricant, causing contact line pinning that dominates the resistance [37,38,194]. As an inviscid droplet oleoplanes at a velocity V, it entrains micrometer-thick lubricant of viscosity μ_o, and as a result, its slide is resisted by a viscous drag associated with Landau–Levich–Derjaguin flow [38,194–198]. The front meniscus of the droplet can be divided into three regions, including the static meniscus, the entrained oil film with thickness h, and the dynamic meniscus connecting the two (Fig. 11d). A pressure

Please cite this article in press as: X. Tang et al., Materials Today, (2020), https://doi.org/10.1016/j.mattod.2020.08.013

TABLE 2

Representative examples of droplets transports.

Mechanism	Method	Force type	Environment	Maximum instantaneous speed (mm s^{-1})	Maximum continuous speed (mm s^{-1})	Limitation	Reference
Gradient surface	Chemical gradient	Capillarity	Solid/air	/	1–2	Trade-off between transport distance and velocity	[205]
	Chemical gradient on microgrooves	Capillarity	Solid/air	60	3.4		[207]
	Chemical gradient on graphene	Capillarity	Solid/air	/	0.04		[208]
	Chemical gradient on carbon nanotube	Capillarity	Solid/air	/	22		[209]
	Chemical gradient	Capillarity	Solid/air	431	144		[210]
	Topographic gradient	Capillarity	Solid/air	/	62.5		[211]
	Topographic gradient	Capillarity	Solid/air	/	40		[214]
	Topographic gradient	Capillarity	Solid/air	/	29.8		[215]
Guiding paths	Engraved track	Gravitational	Solid/air	143	140	Transports lack real-time customization	[173]
	Biphilic path	Gravitational	Solid/air	/	69		[174]
	Biphilic path	Drag	Solid/air	12	/		[220]
	Biphilic path	Gravitational	Solid/air	/	107.6		[222]
Asymmetric stimuli	Asymmetric wettability	Capillarity	Solid/air	/	0.05	Precise steering is difficult	[226]
	Asymmetric roughness	Capillarity	Lubricant/air	/	900		[227]
	Asymmetric temperature	Thermocapillary	Lubricant/air	/	6		[228]
	Asymmetric temperature	Thermocapillary	Liquid bath/air	27	/		[229]
	Asymmetric temperature	Thermocapillary	Lubricant/air	/	9		[230]
	Asymmetric temperature	Thermocapillary	Liquid bath/air	80	5.5		[231]
	Asymmetric height	Gravitational	Liquid bath/air	2	1		[232]
	Asymmetric temperature	Thermocapillary	Lubricant/air	/	1.47		[233]
Potential wells	Magnetic potential well	Magnetic	Lubricant/air	/	0.7	The addressability is limited	[179]
	Magnetic potential well	Magnetic	Liquid bath/air	/	30		[235]
	Gravitational potential well	Gravitational	Solid/air	/	80		[239]
	Gravitational potential well	Gravitational	Solid/air	/	79		[240]
	Electric potential well	Electric	Solid/air	/	1		[242]

match between the dynamic and static meniscus gives the dynamic meniscus length $l \sim \sqrt{Rh/2}$ [38,199]. In the dynamic meniscus, the surface tension withstands the viscous-stress-prompted deformation, and thereby, a balance between the two forces yields the thickness of the entrained oil film, $h \sim R\mathrm{Ca}^{2/3}$, where Ca is the capillary number $\mu_o V/\gamma_{lo}$. As a result, the viscous drag $F_\mu \sim \mu_o Vl\pi w/h \sim \pi\gamma_{lo} w\mathrm{Ca}^{2/3}$ balances the driving force, determining the stable sliding velocity. Because of the complex liquid-infused surface system, different analyses on the droplet mobility have also been reported [200].

As the encapsulating particle shell separates the inner fluid from external contacts, the LMs behave like soft solids (Fig. 11e). LMs with sizes smaller than the capillary length $l_c = \sqrt{\gamma/\rho g}$ maintain quasi-spherical shapes with a contact radius of $w \sim R^2/l_c$ [13]. The rolling of viscous LMs at a low Reynolds number can be well predicted by the Mahadevan–Pomeau regime, where viscous dissipation at the contact zone balances the driving (Fig. 11f) [13,201]. However, for inviscid liquid such as water marbles, such theoretical predictions are limited [39]. It is found that the size and roughness of the coating particles play

Please cite this article in press as: X. Tang et al., Materials Today, (2020), https://doi.org/10.1016/j.mattod.2020.08.013

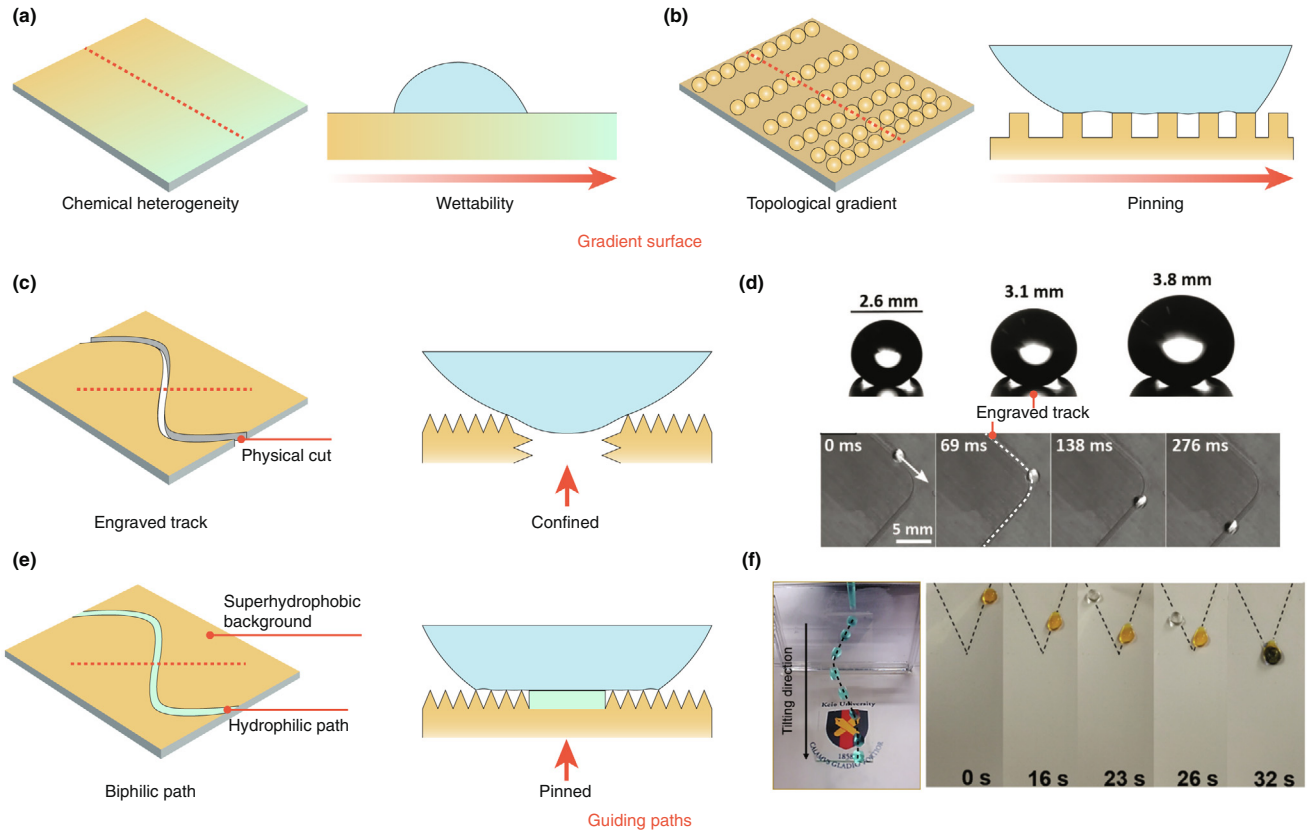

FIGURE 12

Passive transport. (a) On chemically heterogeneous surfaces, droplets tend to move towards regions of high wettability. (b) On surfaces with a topological gradient, droplets tend to move towards strong-pinning regions. (c) Perspective (left) and cross-sectional (right) view of engraved superhydrophobic track. The cross-sectional view is obtained by cutting along red dashed line. Droplets are locally confined within tracks, enabling transport along predefined trajectories. (d) Droplets transport on superhydrophobic tracks whose position is denoted by white dashed line. (e) Perspective (left) and cross-sectional (right) view of biphilic path. On the non-wetting background, pre-patterned paths of high liquid affinity constrain and guide droplet motions. (f) Predefined droplets transport guiding paths patterned with different chemistries. The paths are denoted by black dashed lines. Panel (d) is reprinted with permission from Ref. [173], Wiley-VCH. Panel (f) is reprinted with permission from Ref. [222], American Chemical Society.

a role in the LM motions [202,203]. Large and rough powders tend to increase the friction and thereby decrease the motion speed. Thus, the contacts between shells and substrates start to become important when viscous dissipation is not a dominant factor.

On ideal SLIPSs, droplets creep once they are subjected to even infinitesimal actuations. Unlike such frictionless contacts, threshold forces should be surpassed to initiate the motions for LMs or droplets on SHSs [185,203]. The stable motions also differ. For comparison, we consider scenarios where 10-μl droplets freely descend on 15°-titled-substrates. On SLIPSs, the on-plane gravity component and viscous drag are quickly balanced, resulting in a steady velocity with a magnitude that inversely depends on the lubricant viscosity [38,194]. For LMs and droplets on SHSs, rolling accelerates at a very high rate ($\sim$0.1 m s^{-2}) because of the weak friction and substrate pinning. Such acceleration meets a cut-off as the wind drag and viscous dissipation counteract the gravity, reaching a terminal droplet velocity as high as meters per second [185,204]. Thus, compared with SLIPSs, the SHSs and LMs provide droplets with high but difficult-to-control mobility. By contrast, the droplet velocities on SLIPSs can be readily stabilized and flexibly tuned through the lubricant viscosity.

Passive transport. On-plane droplets transport has attracted broad attention, as Chaudhury et al. demonstrated that water can autonomously ascend a slanted surface patterned with chemical gradients (Table 2) [205]. The driving force derives from the gradient of work of adhesion and is expressed as $\pi w^2\gamma(d\cos\theta/dx)$ [206], where x is the gradient-directional surface position. Such wettability gradients are sculpted through chemical/topographical anisotropy [205,207–216] and unidirectionally or radially distributed (Fig. 12a and b) [205,216]. As droplets are placed, they tend to move towards the region of higher surface energy. However, there is a trade-off between the velocity and range as they oppositely relate to wettability steepness. As a result, to counteract the CAH resistance, the wettability gradient should surpass a threshold value, leading to a transporting range on the order of several millimeters [208–211,213–215], tempering the practical application of such methods. Furthermore, the transport directions cannot be diversified because of the fabrication difficulties, thereby, droplets are only demonstrated to move in either unidirectional or centripetal manners (Table 3).

Please cite this article in press as: X. Tang et al., Materials Today, (2020), https://doi.org/10.1016/j.mattod.2020.08.013

TABLE 3

A summary of the symbols.

θ	Intrinsic contact angle
θ_a	Advancing contact angle
θ_r	Receding contact angle
$\Delta\theta$	Contact angle hysteresis
θ_{app}	Apparent contact angle
θ^m	Microscale contact angle; localized contact angle on microposts
θ^n	Nanoscale contact angle
γ	Surface tension
γ_{ij}	Interfacial tension between phases i and j
f_s	Solid fraction
r	Roughness
a	Diameter of post
τ	Pitch of post
b	Height of post
s	Perimeter of post
l_{app}	Apparent contact line
ϕ	Pinned fraction
D	Inner diameter of channel
R	Radius of droplet
Ω	Volume of droplet
w	Contact radius between droplet and substrate
δ	Sag depth of liquid/vapor interface
l	Length of dynamic meniscus
h	Thickness of entrained lubricant film
l_c	Capillary length
F	Force
F_{adh}	Adhesive force
W	Work of adhesion
U	Potential energy
g	Gravitational acceleration
ΔP	Laplace pressure difference; pressure difference
ΔP_c	Critical pressure
m	Mass
ρ	Density
μ	Viscosity
V	Velocity
S	Spreading coefficient
A	Hamakar constant
x	Position
B	Bending modulus
T	Temperature

To enrich the delivery routes, curved and branched paths have been fabricated on SHSs as well as SLIPSs to guide droplet motions under unidirectional actuations such as gravities and wind drags (Fig. 12c and e) [173,174,217–222]. Unlike the frictionless backgrounds, the paths can pin or confine droplets to prevent the derailment caused by the unaligned direction between the actuation and paths. The driving forces along the railway are difficult to control. Mertaniemi et al. first engraved guiding tracks on SHSs to transport aqueous droplets (Fig. 12d) [173]. Droplets were confined within the grooves and guided along the trajectories at a speed as high as 140 mm s^{-1} [173]. Apart from physical confinements, railways patterned through contrasting chemistries have also been widely reported (Fig. 12e) [174,217,218,220,221]. The most common form is the biphilic surface consisting of SH backgrounds and hydrophilic/hydrophobic paths [174,220,221]. To make the transport of organic liquid possible, the guiding-path strategy is also combined with SLIPSs. While maintaining the background intercalating lubricant layers, the paths are modified to have either high liquid affinity or low porosity to build more droplet/substrate contacts [217–219]. However, the above partial-wetting railways of biphilic surfaces retain a trail of liquid, incurring potential cross-contaminations once the droplets are laden with different reagents. The dynamically omniphobic paths are fabricated to tackle the issues [222]. Such surfaces are fabricated by covalently attaching flexible hydrophobic molecular chains onto smooth substrates [223–225]. Tenjimbayashi et al. used two types of dynamically omniphobic chemistries to programme a repellent surface consisting of a path grafted with a higher surface energy type (Fig. 12f) [222]. As evidenced through energy-dispersive X-ray spectroscopy, the railways retained no detectable residues.

For the aforementioned passive methods, once the surfaces have been fabricated, the motion directions are finalized and velocities can be tuned with limited adjustments. The lack in flexibility and sophistication make them unsuitable to customize delivery in real time. However, droplets can undergo passive transport without external energy input. Such unique benefits make them preferential in fields where continuous droplet removal and delivery is required. For example, Daniel et al. adopted gradient surfaces in heat exchangers; thus, the originally random motions of condensates can be radially biased to improve the heat transfer coefficient [216]. Shin et al. utilized superhydrophobic tracks to successively deliver analytes below detecting lasers, enabling high-throughput surface-enhanced Raman scattering sensing [87]. Thus, the preprogramed and embedded navigations feature autonomous transport usually at high frequency.

Active transport. To actively drive droplets with unlimited freedom, asymmetric contexts, including wettability, surface roughness, and thermal conditions, are frequently imposed on two sides of droplets (Fig. 13) [226–233]. Asymmetric stimuli, including attenuated light, the gradient of the magnetic field or heat, trigger such unbalanced conditions in a dynamic and reconfigurable manner. Thus, on/off of the asymmetric stimuli can drive/brake droplet motions with directions that can be arbitrarily steered by axially rotating the stimuli.

As mentioned above, wettability gradient enables droplet transport within short ranges. To actively modulate the navigation in such a scenario, Ichimura et al. grafted photoresponsive molecules onto a smooth surface, allowing reversible wettability switching upon UV or blue light irradiation (Fig. 13c) [226]. By tuning the direction and steepness of the attenuated light, a wettability gradient can be patterned *in situ*, fuelling on-demand motions. However, the transport velocity is very low ($\sim$35 μm s^{-1}) because of the long response time ($\sim$10 s) and moderate change in wettability ($\sim$10°).

Tian et al. triggered rapidly responsive roughness through a magnetic field gradient to enable fast transport (Fig. 13d) [227]. By impregnating ferrofluid lubricant into a surface grown with a ZnO nanoarray, they fabricated a dynamic SLIPS, which formed self-assembled lubricant microstructures as perpendicular magnetic fields were exerted. The droplets' apparent contact angles depend on the structural amplitudes, the magnitudes of which can be modulated through field intensities. When a gradient field is present, the asperities appear asymmetric, producing unbalanced driving capillary forces. Along with the translation of

Please cite this article in press as: X. Tang et al., Materials Today, (2020), https://doi.org/10.1016/j.mattod.2020.08.013

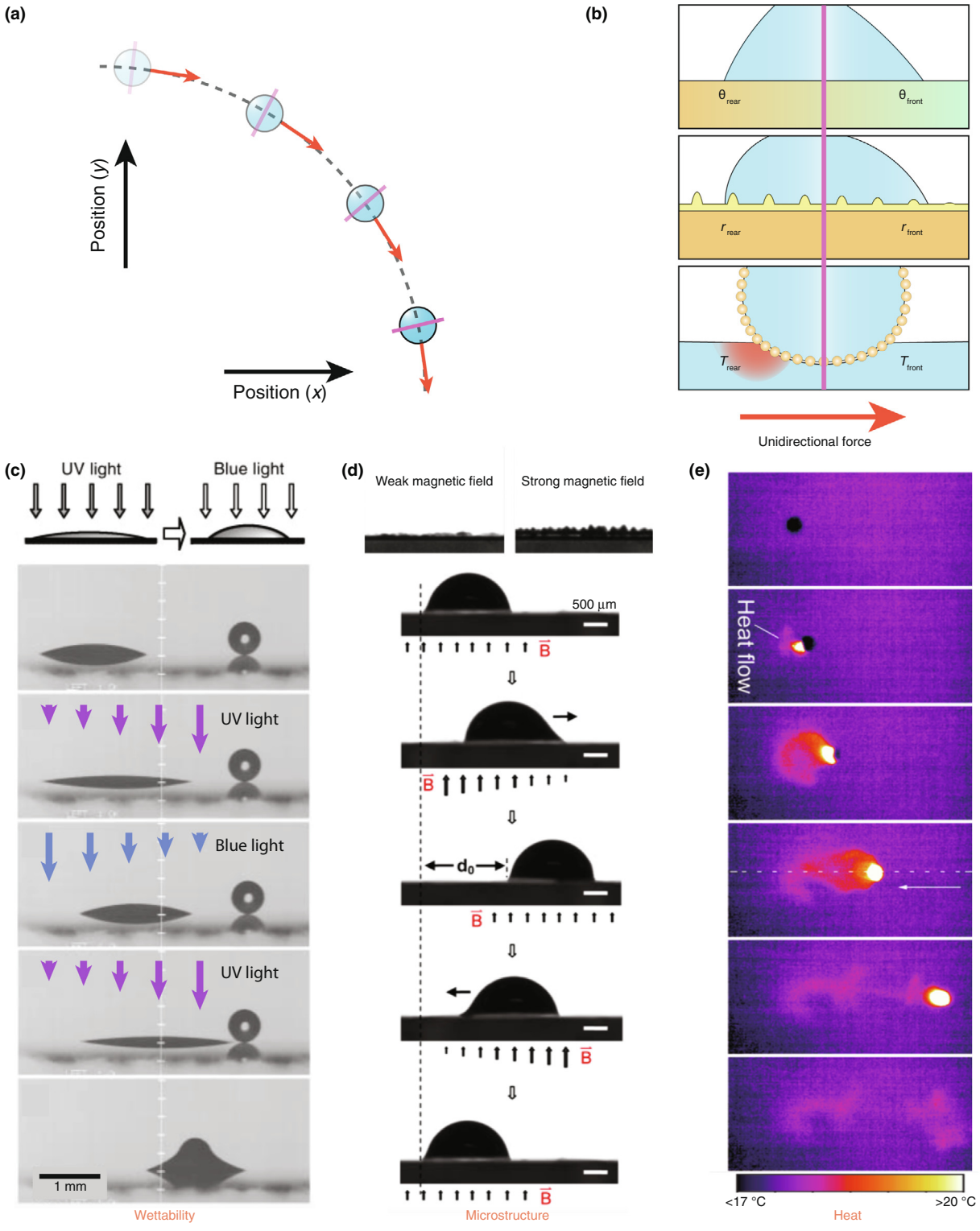

FIGURE 13

Asymmetric active transport. (a) Using the asymmetric method, the bilateral asymmetry has to be directed in real time to navigate droplet motions. (b) The contrasting conditions imposed on the two sides of the droplets trigger unidirectional forces. (c) Droplet motions caused by the wettability gradient, which are *in situ* patterned through photo-responsive chemicals; UV light and blue light, respectively, enhance and reduce liquid affinity of the surface. (d) Asymmetric surface microstructures induce droplet motions on SLIPSs; structural amplitude of the ferrofluid microstructures is determined by the magnetic field strength, thus its gradient field produces asymmetric microstructures. (e) Heterogeneous heating creates Marangoni forces to drive liquid marbles on water surfaces. Panel (c) is reprinted with permission from Ref. [226], American Association for the Advancement of Science. Panel (d) is reprinted with permission from Ref. [227], American Chemical Society. Panel (e) is reprinted with permission from Ref. [229], Wiley-VCH.

Please cite this article in press as: X. Tang et al., Materials Today, (2020), https://doi.org/10.1016/j.mattod.2020.08.013

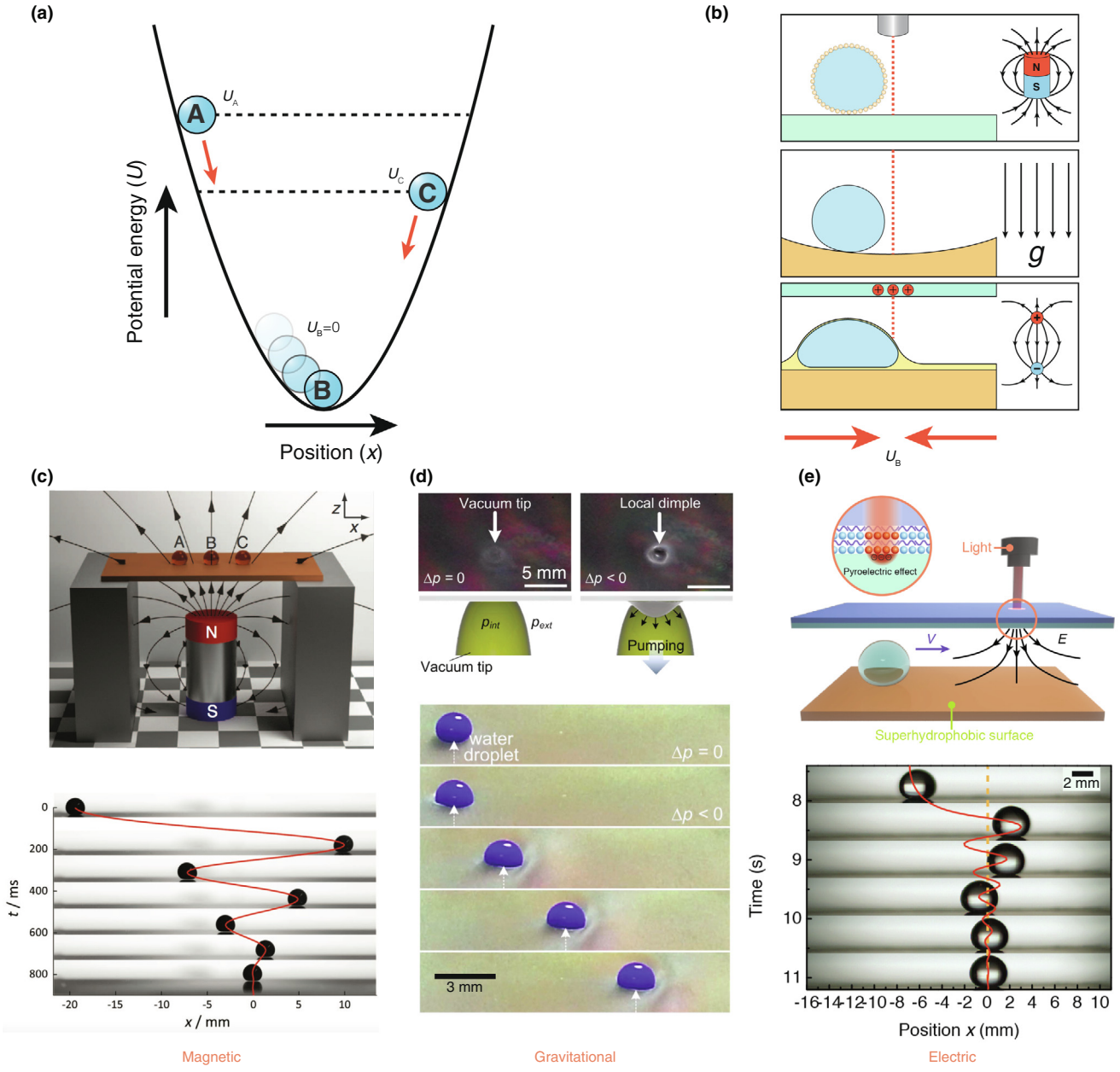

FIGURE 14

Active transport through potential wells. (a) Using the potential well method, droplets are actuated towards and finally immobilized at the position of minimum potential energy. Images are adopted from Ref. [260], Nature Publishing Group. (b) Magnetic, electric, and gravitational potential wells precisely position droplets within their effective range. (c) The magnetic potential well attracts nearby magnetic droplets on SHSs. (d) Geometric dimples trap and convey droplets across elastic SHSs. (e) Light-triggered electric fields position droplets below light spots on SHSs through dielectrophoretic forces. Panel in (c) is reprinted with permission from Refs. [260,261], Nature Publishing Group and Wiley-VCH. Panel (d) is reprinted with permission from Ref. [237], Nature Publishing Group. Panel (e) is reprinted with permission from Ref. [242], American Chemical Society.

in situ formed asperities, droplets are reported to move at a maximum speed of 0.9 m s^{-1}. The rapid and reconfigurable pattern formation is a unique properties materialized through the highly deformable ferrofluid.

The thermal gradient is also utilized to transport droplets. A special case is the LM transport on a water bath [229,231]. Paven et al. coated cargo droplets with hydrophobic photothermal materials, enabling thermogenesis upon near infrared irradiation (Fig. 13e) [229,231]. As the illumination is focused on one side of the LMs, local heating raises the temperature, which in turn decreases the surface tension γ of nearby water. Thereby, a Marangoni force of roughly $2R\Delta\gamma$ starts to drive the LMs towards unirradiated sides. The instantaneous acceleration can reach ~0.1 m s^{-2} [229]. As a result, the light faces difficulty in precisely moving along with the LMs, causing pulsed driving and subsequently discontinuous motions.

The driving forces of such asymmetric methods are derived from the contrast of the bilateral conditions. As droplets move, such spatial asymmetry has to follow to provide constant propulsions. To steer droplets along particular trajectories, the asymme-

Please cite this article in press as: X. Tang et al., Materials Today, (2020), https://doi.org/10.1016/j.mattod.2020.08.013

try has to be constantly redirected. As a result, the required performing skills appear to be demanding and complex (Fig. 13a). An overlooked prerequisite is the sufficient droplet/substrate contacts, which basically precludes SHSs from such methods because of their finite liquid/solid interface. The contrast, reversibility, responsive speed, and accompanying capability of the triggering asymmetry jointly govern the performance of the transports.

Unlike the asymmetry method, an alternative active counterpart creates potential wells towards which droplets follow (Fig. 14). In the droplet vicinity, a well of potential, including gravitational, electric, and magnetic types, is generated, and the droplet immediately converts its potential energy into kinetic energy and moves towards the position of the minimum energy state (Fig. 14b) [64,179,234–242]. In this way, the continuous presence of the potential well can immobilize and position droplets within it rather than bringing them into continuous motion like the asymmetric method. By simply controlling the speed and trajectories of the potential well, droplets can be precisely navigated across the surface.

Magnetic potential wells are usually achieved by placing an axially magnetized cylindrical magnet above or under the platform (Fig. 14c). Droplets are made magnetically responsive through either magnetic nanoparticles doping or hydrophobic magnetic particle coating [180,243]. On SHSs, the magnetic-nanoparticles-laden droplets follow the magnet motions [180]. Similarly, using the same method, the magnetic LMs can also be remotely handled on varied surfaces, including hydrophilic or water surfaces [64,234–236]. The magnetic nanoparticles can also be doped into the lubricant, causing the SLIPSs to become magnetically active [179]. Droplets placed on the SLIPSs are cloaked within the ferrofluid lubricant and, thus, can be attracted towards the magnetic potential well. However, such doping or coating methods inevitably contaminate the droplets, biasing the reaction or detection results.

To circumvent these issues, gravitational potential wells are utilized to handle droplets on SHSs [237–241]. The gravitational potential wells are commonly achieved by dimpling the elastic and deformable SHSs (Fig. 14d). Seo et al. and Han et al. respectively created local craters through magnetic attraction on magnetically functionalized soft superhydrophobic substrates or vacuum-tip-induced suction on elastic superhydrophobic films [239,241]. A droplet near the dimple rolls on the downward slope and is immobilized inside the geometric base. The movement of dimples directly controls droplet motions, and fast motion at 80 mm s^{-1} has been achieved [239].

The electric potential well is another form of energy to manipulate droplets. As demonstrated in a platform termed "pyroelectro-trapping on superhydrophobic surfaces", using a pyroelectric crystal, the electric potential well can be realized without voltage sources and electric circuits (Fig. 14e) [242]. By integrating the pyroelectric crystal with a photothermal material, a locally non-uniform electric field can be generated through near infrared laser irradiation. In this way, droplets on either SHS or SLIPS can be driven and positioned right under the light spot, offering light-controlled droplets transport in a loss-free manner. Because the spatial position of light can be readily controlled by optical system without the need for moving parts, light-controlled methods are more suitable for future automatic systems.

For potential-well methods, droplet positions can be readily guided by single stimuli, ignoring complex navigations associated with the asymmetry methods. However, the manipulation addressability is somehow impaired as droplets within the well indiscriminatingly react and move towards the centre positions. The strength, steepness, and spatial range of the potential well work in concert to dictate the performance. In contrast to the asymmetry methods where stimuli have to follow the droplets, the stimuli actually guide the motion of droplets in potential well methods. However, a maximum maneuverable velocity exists beyond which droplets cannot catch up with the leading traps. However, a systematic investigation on such maximum velocity is still lacking.

Perspective

As a wide spectrum of industrial applications and scientific studies involve the participation of liquids, the possibility of manipulating liquids in a manner similar to the handling of solid objects has attracted broad interests. The manoeuvring precision, dexterity, and efficiency remarkably influence the synthetic products and analytical results. In this review, we focus on three fundamental aspects of droplet manipulation: the aliquot, grip, and transport of tiny droplets. The nature of liquid/solid contact differentiates the handling of liquids from that of solids and yields issues such as the spreading, retention, and sticking of liquids. Retention-proof approaches such as SHSs, SLIPSs, and LMs provide solutions to the aforementioned issues, and their applications in liquid manoeuvring have unlocked unprecedented capabilities that have brought about unique performances in various applications.

On the basis of reported works, several key points can be concluded for different facets of liquid manipulation. For aliquoting, performance limitation is characterized by the attainable minimum droplet volume. The producible critical volume is remarkably determined by the sizes of key features, such as the inner diameters of 1D channels and areas of 2D patches. For grip, the liquid/solid adhesion defines the manipulating capability. Such adhesion originates from the micro-capillary bridges, with individual and collective behaviors that play critical roles. SHSs are the main workhorse in aliquot and grip. SLIPSs and LMs widely participate in droplet transport. Although through the use of SLIPSs and LMs, the droplet volume can be well preserved, additional lubricant or hydrophobic powders will contaminate the droplet surfaces. Sometimes, such encasing layers are considered beneficial because of the isolation of inner fluids from surrounding environments, reducing the evaporation speed and retarding the reaction rate. The active navigation of droplet motions, including their speeds and directions, is the key transport features and often controlled by external stimuli. To make the system stimulus-responsive, either bulky or interfacial functionalization towards substrates of SHSs, substrates/lubricants of SLIPSs, and substrate/shells of LMs are necessary. The stimuli and functionalization work in concert to transport droplets. Techniques such as pyroelectro-trapping on superhydrophobic surfaces circumvent the need for such

Please cite this article in press as: X. Tang et al., Materials Today, (2020), https://doi.org/10.1016/j.mattod.2020.08.013

functionalization, providing adaptable solutions that work for most common non-wetting interfaces [242].

The aforementioned strategies usually grip and transport micro-to-nano-liter droplets, leaving the lower volume extremum unexplored. The smallest size for manipulation is bounded by the liquid volume limit toward which the retention-proof interfaces are still effective. For SHSs, nano-textured types such as mosquitoes' eyes can repel fog droplets of 10 μm in diameter [244]. For SLIPSs, 100-μm condensates become highly mobile aloft the lubricant [245]. The LMs are typically millimeter-sized because of the coating difficulties on micrometer droplets. However, unconventional techniques such as industrial mixer agitations and water condensations are shown to enable microfabrication of LMs of ~20 μm in diameter which remain mobile on solids [246,247]. Before the potentials can be fully exploited, several issues remain unsolved. For example, in ambient environment, such small droplets tend to quasi-instantaneously evaporate in ~100 ms, demanding for the careful control of temperature as well as humidity to prolong their lifetime. Moreover, the controlling stimuli for transport should be downsized to ~1 μm to precisely address individual droplet. The loss-free manipulation of microscale and even nanoscale liquids merits abundant technological prospects, yet remains a challenge using current strategies.

Many opportunities still remain for exploration. The production rate of free droplets in the quasi-static manner is still low. High-throughput of such quasi-static aliquoting may introduce new features for various fields, including 3D printing processes. For grip, adhesion switching contrast must be improved so that droplets of broader volume ranges can be handled. The switching quality needs to be highlighted, as *in situ*, rapid, and reversible switching is key to real-time manipulation. New designs and strategies remain necessary to improve the grip sophistication, such as an independent adhesion switching on different regions of a single surface. For transport, a common set of performance metrics still needs to be considered for evaluation and comparison of different techniques. Apart from droplet navigations, features such as the transportable spatial range and droplet addressability are key in practical applications but rarely considered. The reported transports are commonly performed on horizontal and planar surfaces, and transports on tilted or even curved surfaces can enrich our handling capability and may be significant for fields such as stretchable electronics. The use of an SHS-/LM-based method for manipulation is usually limited to high-surface-tension liquids such as water and glycerol. Low-surface-tension fluids such as alcohols, alkanes, and silicone oils tend to impregnate the micro-/nano-scale textures and spread on the surface, thus increasing the CAH significantly. As a result, droplets experience substantial resistances, defying their ready transports. With advances in superoleophobic surfaces [248,249], the manipulation of low-surface-tension fluids has been reported [70,71,234,250,251]. Additional investigations are required to extend the current approaches to handle a wide variety of liquids.

Moreover, the manipulation strategies can potentially be adapted for other fluidized materials such as liquid metals. Because of benefits such as nontoxicity, low vapor pressure, excellent electrical and thermal conductivity, the gallium-based liquid metal alloys such as eutectic gallium-indium (EGaIn) and gallium-indium-tin (Galinstan) widely participate in various microdevices, including switches, valves, pumps, and sensors, wherein their manipulations play key roles [252]. Unlike common liquids, the liquid metals instantaneously form 1–3 nm thick oxide skin in air, making them sticky on almost any surfaces [253]. To effortlessly handle liquid metals without residues, similar retention-proof techniques have been developed. For example, by simply texturing surfaces regardless of their surface energies (nonreactive to liquid metals), the micro-/nano-structures can suspend liquid metals in Cassie states, forming "oxide-phobic" surfaces [254,256]. On porous surfaces infused with hydrochloric acid, the oxide skins of liquid metals can be dissolved, restoring their pristine metal surfaces with surface tension of ~500–600 mN m^{-1} [257]. In this way, the liquid metals bead up and freely roll, reminiscent of droplets on SLIPSs. Similarly, by rolling the liquid metal droplets over a powder bed, micro-/nano-particles can be coated over the liquid metals. Such liquid metal marble is mobile on solid surface and even can float on water surfaces [258,259]. Although the retention-proof interfaces have been adapted for liquid metals, delicate manipulation strategies still remain to be adopted. Such capability may promote new advances for applications such as reconfigurable electronics and energy harvesting.

Because they effectively suppress wetting and spreading, retention-proof interfaces pave the way for loss-free droplet handling and manipulation. Every technique has its own limitation in certain aspects of liquid manipulation. Understanding the strengths and weaknesses of various approaches can potentially enable us to combine the benefits of diverse strategies. Dexterous and lossless liquid manoeuvring enriches our interactions with liquids and broadens further explorations in various fields in which liquids play a critical role.

Declaration of Competing Interest

The authors declare that they have no known competing financial interests or personal relationships that could have appeared to influence the work reported in this paper.

Acknowledgements

The financial support from the Research Grants Council of Hong Kong (GRF 17204420, 17210319, 17204718 and 17237316; CRF C101817G) is gratefully acknowledged. This work was also supported in part by the Zhejiang Provincial, Hangzhou Municipal and Lin'an County Governments.

Author contributions

L.W. supervised the project. X.T. conceived the idea and designed the review. X.T. and L.W. wrote the review. All authors discussed the review and commented on the manuscript.

References

[1] A. Bicchi, IEEE Trans. Robot. Autom. 16 (6) (2000) 652.
[2] D.G. Grier, Nature 424 (6950) (2003) 810.
[3] A. Ashkin et al., Nature 330 (6150) (1987) 769.
[4] M.P. MacDonald et al., Nature 426 (6965) (2003) 421.
[5] G. Vieira et al., Phys. Rev. Lett. 103 (12) (2009) 128101.
[6] J. Yan et al., Phys. Rev. E 70 (1) (2004) 011905.
[7] H. Lee et al., Appl. Phys. Lett. 85 (6) (2004) 1063.

Please cite this article in press as: X. Tang et al., Materials Today, (2020), https://doi.org/10.1016/j.mattod.2020.08.013

[8] F.J. Rubio-Sierra et al., Adv. Eng. Mater. 7 (4) (2005) 193.
[9] L. Kremser et al., Electrophoresis 25 (14) (2004) 2282.
[10] C.R. Cabrera, P. Yager, Electrophoresis 22 (2) (2001) 355.
[11] M.P. Hughes, Electrophoresis 23 (16) (2002) 2569.
[12] T. Hunt, R. Westervelt, Biomed. Microdevices 8 (3) (2006) 227.
[13] P. Aussillous, D. Quéré, Nature 411 (6840) (2001) 924.
[14] Y. Zhao, K. Chakrabarty, IEEE Trans. Comput.-Aided Des. Integr. Circuits Syst. 31 (6) (2012) 817.
[15] A. Lafuma, D. Quéré, Nat. Mater. 2 (7) (2003) 457.
[16] W. Barthlott, C. Neinhuis, Planta 202 (1) (1997) 1.
[17] L. Feng et al., Adv. Mater. 14 (24) (2002) 1857.
[18] H.J. Ensikat et al., Beilstein J. Nanotechnol. 2 (1) (2011) 152.
[19] T.-S. Wong et al., Nature 477 (7365) (2011) 443.
[20] H.F. Bohn, W. Federle, PNAS 101 (39) (2004) 14138.
[21] N. Pike et al., Proc. R. Soc. Lond., B Biol. Sci. 269 (1497) (2002) 1211.
[22] T. Young, Philos. Trans. R. Soc. 95 (1805) 65.
[23] J.W. Gibbs, Trans. Connect. Acad. Arts Sci. 3 (1878) 343.
[24] H. Eral, J. Oh, Colloid Polym. Sci. 291 (2) (2013) 247.
[25] R. Tadmor, Langmuir 20 (18) (2004) 7659.
[26] J. Joanny, P.-G. De Gennes, J. Chem. Phys. 81 (1) (1984) 552.
[27] L. Gao, T.J. McCarthy, Langmuir 22 (14) (2006) 6234.
[28] A. Cassie, Discuss. Faraday Soc. 3 (1948) 11.
[29] A. Cassie, S. Baxter, Trans. Faraday Soc. 40 (1944) 546.
[30] R.N. Wenzel, Ind. Eng. Chem. 28 (8) (1936) 988.
[31] R.N. Wenzel, J. Phys. Chem. 53 (9) (1949) 1466.
[32] P. Roach et al., Soft Matter 4 (2) (2008) 224.
[33] Y. Kwon et al., Langmuir 25 (11) (2009) 6129.
[34] C. Lee, C.-J.-C. Kim, Langmuir 27 (7) (2011) 4243.
[35] M. Miwa et al., Langmuir 16 (13) (2000) 5754.
[36] J.B. Boreyko et al., Proc. Natl. Acad. Sci. U.S.A. 111 (21) (2014) 7588.
[37] J.D. Smith et al., Soft Matter 9 (6) (2013) 1772.
[38] X. Tang et al., ACS Appl. Mater. Interfaces (2018).
[39] Aussillous, P., and Quéré, D., Proc. R. Soc. London, Ser. A (2006) 462 (2067), 973.
[40] G. McHale, M.I. Newton, Soft Matter 7 (12) (2011) 5473.
[41] E. Bormashenko, Curr. Opin. Colloid Interface Sci. 16 (4) (2011) 266.
[42] R. Blossey, Nat. Mater. 2 (5) (2003) 301.
[43] R. Fürstner et al., Langmuir 21 (3) (2005) 956.
[44] B. Bhushan, Y.C. Jung, Prog. Mater Sci. 56 (1) (2011) 1.
[45] B. Bhushan et al., Langmuir 25 (5) (2009) 3240.
[46] A.K. Epstein et al., PNAS 109 (33) (2012) 13182.
[47] L. Xiao et al., ACS Appl. Mater. Interfaces 5 (20) (2013) 10074.
[48] X. Hou et al., Nature 519 (7541) (2015) 70.
[49] J. Li et al., ACS Appl. Mater. Interfaces 5 (14) (2013) 6704.
[50] K. Watanabe et al., J. Fluid Mech. 381 (1999) 225.
[51] R. Truesdell et al., Phys. Rev. Lett. 97 (4) (2006) 044504.
[52] Z. Ming et al., Soft Matter 7 (9) (2011) 4391.
[53] S.Y. Teh et al., Lab Chip 8 (2) (2008) 198.
[54] M. Srisa-Art et al., Anal. Chem. 79 (17) (2007) 6682.
[55] J.R. Dorvee et al., Nat. Mater. 3 (12) (2004) 896.
[56] O.D. Velev et al., Nature 426 (6966) (2003) 515.
[57] V. Srinivasan et al., Lab Chip 4 (4) (2004) 310.
[58] I. Barbulovic-Nad et al., Lab Chip 8 (4) (2008) 519.
[59] P.S. Dittrich, A. Manz, Nat. Rev. Drug Discov. 5 (3) (2006) 210.
[60] A.B. Theberge et al., Angew. Chem. Int. Ed. 49 (34) (2010) 5846.
[61] R. Karnik et al., Nano Lett. 8 (9) (2008) 2906.
[62] H.M. Wyss et al., Phys. Rev. E 74 (6) (2006) 061402.
[63] M. Abdelgawad, A.R. Wheeler, Adv. Mater. 21 (8) (2009) 920.
[64] Y. Zhao et al., Adv. Funct. Mater. 25 (3) (2015) 437.
[65] S.D. Hoath, Fundamentals of Inkjet Printing: The Science of Inkjet and Droplets, John Wiley & Sons, 2016.
[66] E.R. Lee, Microdrop Generation, CRC Press, 2002.
[67] R. Suryo, O.A. Basaran, Phys. Rev. Lett. 96 (3) (2006) 034504.
[68] Z. Dong et al., ACS Nano 7 (11) (2013) 10371.
[69] Y. Mao et al., Lab Chip 18 (18) (2018) 2720.
[70] L. Wu et al., Small 11 (37) (2015) 4837.
[71] W.S. Wong et al., Small 13 (14) (2017) 1603688.
[72] W.S. Wong et al., ACS Nano 11 (1) (2017) 587.
[73] E. Ueda et al., Lab Chip 12 (24) (2012) 5218.
[74] H. Li et al., ACS Appl. Mater. Interfaces 7 (17) (2015) 9060.
[75] D. Paulssen et al., Adv. Mater. Interf0aces 5 (18) (2018) 1800852.
[76] P.M. Reis et al., Soft Matter 6 (22) (2010) 5705.
[77] S. Jung et al., Phys. Fluids 21 (9) (2009) 091110.
[78] M. He et al., Adv. Funct. Mater. (2018) 1800187.
[79] Q. Meng et al., NPG Asia Mater. 6 (9) (2014) e125.
[80] Y.L. Han et al., Adv. Funct. Mater. 27 (22) (2017) 1606607.
[81] X. Tang et al., Nat. Commun. 8 (2017) 14831.
[82] S. Wooh et al., Adv. Mater. 27 (45) (2015) 7338.
[83] V. Rastogi et al., Adv. Mater. 20 (22) (2008) 4263.
[84] V. Rastogi et al., Macromol. Rapid Commun. 31 (2) (2010) 190.
[85] F. De Angelis et al., Nat. Photonics 5 (11) (2011) 682.
[86] H. Zhao et al., J. Mater. Chem. A 3 (8) (2015) 4330.
[87] S. Shin et al., Small 13 (2017) 7.
[88] F. Xu et al., J. Phys. Chem. C 115 (20) (2011) 9977.
[89] L. Li et al., Colloids Surf. B 106 (2013) 176.
[90] A.I. Neto et al., Soft Matter 7 (9) (2011) 4147.
[91] M. Liu, L. Jiang, Adv. Funct. Mater. 20 (21) (2010) 3753.
[92] M. Liu et al., Acc. Chem. Res. 43 (3) (2009) 368.
[93] P.-G. De Gennes, Rev. Mod. Phys. 57 (3) (1985) 827.
[94] Y. Sun et al., Surf. Innov. 6 (1–2) (2017) 93.
[95] B. Samuel et al., J. Phys. Chem. C 115 (30) (2011) 14852.
[96] Z. Guo et al., Nanoscale 6 (21) (2014) 12822.
[97] X. Zhang et al., Adv. Sci. 5 (1) (2018) 1700520.
[98] Israelachvili, J. N., Intermolecular and surface forces: revised third edition. Academic press: 2011.
[99] T. Nishino et al., Langmuir 15 (13) (1999) 4321.
[100] P.-G. De Gennes et al., Capillarity and Wetting Phenomena: Drops, Bubbles, Pearls, Waves, Springer Science & Business Media, 2013.
[101] A.T. Paxson, K.K. Varanasi, Nat. Commun. 4 (2013) 1492.
[102] D. Li et al., Soft Matter 12 (18) (2016) 4257.
[103] C. Dorrer, J. Ruehe, Adv. Mater. 20 (1) (2008) 159.
[104] W.K. Cho, I.S. Choi, Adv. Funct. Mater. 18 (7) (2008) 1089.
[105] M. Jin et al., Adv. Mater. 17 (16) (2005) 1977.
[106] D.Y. Lee et al., Soft Matter 8 (18) (2012) 4905.
[107] L. Feng et al., Langmuir 24 (8) (2008) 4114.
[108] W.S.Y. Wong et al., Adv. Mater. Interf. 2 (9) (2015) 1500071.
[109] W.S. Wong et al., Sci. Adv. 2 (6) (2016) e1600417.
[110] D. Wang et al., Colloids Surf. A 538 (2018) 262.
[111] X. Lu et al., Sci. Bull. 60 (4) (2015) 453.
[112] D. Quéré, Annu. Rev. Mater. Res. 38 (2008) 71.
[113] A. Winkleman et al., Nano Lett. 8 (4) (2008) 1241.
[114] A. Peters et al., Eur. Phys. J. E 29 (4) (2009) 391.
[115] X. Liu et al., Soft Matter 8 (7) (2012) 2070.
[116] R. Fang et al., Adv. Mater. Interfaces 5 (3) (2018) 1701176.
[117] W. Song, Nanoscale 6 (22) (2014) 13435.
[118] X. Liu et al., Soft Matter 7 (7) (2011) 3331.
[119] C. Li et al., Adv. Mater. 21 (42) (2009) 4254.
[120] X. Liu et al., Soft Matter 8 (40) (2012) 10370.
[121] X. Liu et al., Langmuir 26 (14) (2010) 12377.
[122] Z. Cheng et al., Chem. Asian J. 8 (12) (2013) 3200.
[123] L. Xu et al., Macromol. Rapid Commun. 36 (12) (2015) 1205.
[124] L. Xu et al., Adv. Mater. Interf. 1 (2014) 4.
[125] J.K. Park et al., ACS Appl. Mater. Interfaces 9 (38) (2017) 33333.
[126] J.N. Wang et al., Adv. Funct. Mater. 28 (23) (2018) 1800625.
[127] J. Wang et al., NPG Asia Mater. 10 (2) (2018) e470.
[128] J. Seo et al., Adv. Mater. 25 (30) (2013) 4139.
[129] D. Kim et al., Chem. Mater. 27 (14) (2015) 4964.
[130] Z. Wang et al., Sens. Actuators, B 244 (2017) 649.
[131] C. Yang et al., ACS Appl. Mater. Interfaces 10 (23) (2018) 20150.
[132] Y. Li et al., PNAS 114 (13) (2017) 3387.
[133] E. Bormashenko, Adv. Colloid Interface Sci. 222 (2015) 92.
[134] W. Fang et al., Langmuir 34 (13) (2018) 3838.
[135] C. Li et al., Soft Matter 8 (14) (2012) 3730.
[136] X.D. Zhao et al., Adv. Funct. Mater. 21 (1) (2011) 184.
[137] Z. Cheng et al., Adv. Funct. Mater. 18 (20) (2008) 3219.
[138] G. Hou et al., ACS Appl. Mater. Interfaces 9 (27) (2017) 23238.
[139] W.S. Wong et al., Adv. Funct. Mater. 26 (3) (2016) 399.
[140] D. Wu et al., Adv. Mater. 23 (4) (2011) 545.
[141] X. Hong et al., J. Am. Chem. Soc. 129 (6) (2007) 1478.
[142] D. Guo et al., Small 11 (35) (2015) 4491.
[143] Y. Zhao et al., Adv. Mater. 22 (6) (2010) 707.
[144] C.H. Ooi et al., Microfluid. Nanofluid. 22 (12) (2018) 142.
[145] Y. Lai et al., Langmuir 24 (8) (2008) 3867.
[146] L. Heng et al., J. Mater. Chem. A 3 (47) (2015) 23699.
[147] M. Chen et al., ACS Appl. Mater. Interfaces 9 (27) (2017) 23246.
[148] G. Guangming et al., Soft Matter 10 (4) (2014) 549.

Please cite this article in press as: X. Tang et al., Materials Today, (2020), https://doi.org/10.1016/j.mattod.2020.08.013

[149] J. Huang et al., J. Mater. Chem. A 2 (43) (2014) 18531.
[150] E. Zhang et al., Nanoscale 7 (14) (2015) 6151.
[151] G. Ding et al., J. Mater. Chem. A 5 (33) (2017) 17325.
[152] Y. Wang et al., RSC Adv. 7 (84) (2017) 53525.
[153] Q. Gao et al., RSC Adv. 7 (79) (2017) 50403.
[154] G. Gong et al., Macromol. Mater. Eng. 300 (11) (2015) 1057.
[155] Z. Hu et al., Adv. Funct. Mater. 24 (40) (2014) 6381.
[156] Z. Cheng et al., Nanoscale 5 (7) (2013) 2776.
[157] A. Gao et al., J. Mater. Chem. A 4 (31) (2016) 12058.
[158] T. Zhu et al., ACS Appl. Mater. Interfaces 9 (11) (2017) 10224.
[159] Y. Peng et al., Adv. Mater. Interf. 4 (20) (2017) 1700497.
[160] Z. Cheng et al., ACS Appl. Mater. Interfaces 5 (17) (2013) 8753.
[161] J. Long et al., ACS Appl. Mater. Interfaces 7 (18) (2015) 9858.
[162] G. Gong et al., J. Mater. Chem. 22 (17) (2012) 8257.
[163] A. Gao et al., J. Colloid Interface Sci. 505 (2017) 49.
[164] J. Li et al., Surf Coat Tech. 258 (2014) 973.
[165] J. Li et al., Appl. Surf. Sci. 289 (2014) 1.
[166] Z. Xiong et al., Macromol. Mater. Eng. 301 (6) (2016) 653.
[167] K. Liu et al., Nanoscale 4 (3) (2012) 768.
[168] J. Zhang et al., Soft Matter 4 (11) (2008) 2232.
[169] E. Brouzes et al., PNAS 106 (34) (2009) 14195.
[170] L.B. Pinheiro et al., Anal. Chem. 84 (2) (2011) 1003.
[171] K.T. Kotz et al., J. Am. Chem. Soc. 127 (16) (2005) 5736.
[172] L. Mazutis et al., Nat. Protoc. 8 (5) (2013) 870.
[173] H. Mertaniemi et al., Adv. Mater. 23 (26) (2011) 2911.
[174] J. Seo et al., ACS Appl. Mater. Interfaces 3 (12) (2011) 4722.
[175] M. Washizu, IEEE Trans. Ind. Appl. 34 (4) (1998) 732.
[176] S.K. Cho et al., J. Microelectromech. Syst. 12 (1) (2003) 70.
[177] D.J. Im et al., Anal. Chem. 85 (8) (2013) 4038.
[178] M.J. Jebrail et al., Lab Chip 12 (14) (2012) 2452.
[179] K.S. Khalil et al., Appl. Phys. Lett. 105 (4) (2014) 041604.
[180] Z. Long et al., Lab Chip 9 (11) (2009) 1567.
[181] Y. Zhang, N.-T. Nguyen, Lab Chip 17 (6) (2017) 994.
[182] Y. Koc et al., Lab Chip 8 (4) (2008) 582.
[183] M. Jönsson-Niedziółka et al., Lab Chip 11 (3) (2011) 490.
[184] N. Gao et al., Nat. Phys. 14 (2) (2018) 191.
[185] D. Daniel et al., Phys. Rev. Lett. 120 (24) (2018) 244503.
[186] L. Gao, T.J. McCarthy, Langmuir 22 (7) (2006) 2966.
[187] F. Schellenberger et al., Phys. Rev. Lett. 116 (9) (2016) 096101.
[188] R. Dufour et al., Small 8 (8) (2012) 1229.
[189] D. Quéré, Rep. Prog. Phys. 68 (11) (2005) 2495.
[190] R.H. Ras et al., Droplet Manipulation on Liquid-Repellent Surfaces, in: Non-Wettable Surfaces, 2016, p. 368.
[191] C. Furmidge, J. Colloid Sci. 17 (4) (1962) 309.
[192] E. Dussan, J. Fluid Mech. 151 (1985) 1.
[193] C. Extrand, A. Gent, J. Colloid Interface Sci. 138 (2) (1990) 431.
[194] D. Daniel et al., Nat. Phys. 13 (10) (2017) 1020.
[195] L.D. Landau, B.G. Levich, Acta Physicochim. URSS 17 (1942) 42.
[196] F. Bretherton, J. Fluid Mech. 10 (02) (1961) 166.
[197] J.C. Kao et al., Phys. Fluids 22 (6) (2010) 061705.
[198] B. Derjaguin, Dokl. Acad. Sci. USSR 39 (1943) 13.
[199] P. Aussillous, D. Quéré, EPL (Europhysics Letters) 59 (3) (2002) 370.
[200] A. Keiser et al., Soft Matter 13 (39) (2017) 6981.
[201] L. Mahadevan, Y. Pomeau, Phys. Fluids 11 (9) (1999) 2449.
[202] A.V. Rao et al., J. Colloid Interface Sci. 285 (1) (2005) 413.
[203] S. Imai, Sens. Actuators, A 274 (2018) 73.
[204] T. Mouterde et al., PNAS 116 (17) (2019) 8220.
[205] M.K. Chaudhury, G.M. Whitesides, Science 256 (5063) (1992) 1539.
[206] S. Daniel, M.K. Chaudhury, Langmuir 18 (9) (2002) 3404.
[207] B. Chandesris et al., Colloids Surf. A 434 (2013) 126.
[208] S.C. Hernandez et al., ACS Nano 7 (6) (2013) 4746.
[209] D.J. Babu et al., Adv. Mater. Interf. 1 (2) (2014) 1300049.
[210] T.N. Banuprasad et al., ACS Appl. Mater. Interfaces 9 (33) (2017) 28046.
[211] J. Yang et al., J. Microelectromech. Syst. 15 (3) (2006) 697.
[212] C. Sun et al., Thin Solid Films 516 (12) (2008) 4059.
[213] J. Yang et al., Langmuir 24 (17) (2008) 9889.
[214] J. Li et al., Adv. Mater. Interf. 1 (3) (2014) 1400001.
[215] J. Li et al., Sci. Adv. 2 (6) (2016) e1600148.
[216] S. Daniel et al., Science 291 (5504) (2001) 633.
[217] I. You et al., ACS Nano 8 (9) (2014) 9016.
[218] U. Manna, D.M. Lynn, Adv. Mater. 27 (19) (2015) 3007.
[219] X. Chen et al., ACS Appl. Mater. Interfaces 9 (2) (2017) 1959.
[220] H. Hu et al., Langmuir 32 (29) (2016) 7339.
[221] X. Yang et al., J. Phys. Chem. C 120 (13) (2016) 7233.
[222] M. Tenjimbayashi et al., ACS Appl. Mater. Interfaces 9 (12) (2017) 10371.
[223] D.F. Cheng et al., Angew. Chem. 124 (12) (2012) 3010.
[224] M. Rabnawaz, G. Liu, Angew. Chem. Int. Ed. 54 (22) (2015) 6516.
[225] L. Wang, T.J. McCarthy, Angew. Chem. Int. Ed. 55 (1) (2016) 244.
[226] K. Ichimura et al., Science 288 (5471) (2000) 1624.
[227] D. Tian et al., ACS Nano 10 (6) (2016) 6220.
[228] N. Bjelobrk et al., Phys. Rev. Fluids 1 (6) (2016) 063902.
[229] M. Paven et al., Adv. Funct. Mater. 26 (19) (2016) 3199.
[230] P. Irajizad et al., Adv. Mater. Interf. 4 (12) (2017) 1700009.
[231] H. Kawashima et al., ACS Appl. Mater. Interfaces 9 (38) (2017) 33351.
[232] J. Vialetto et al., Angew. Chem. Int. Ed. 56 (52) (2017) 16565.
[233] C. Gao et al., Adv. Funct. Mater. 28 (35) (2018) 1803072.
[234] Y. Xue et al., Adv. Mater. 22 (43) (2010) 4814.
[235] L. Zhang et al., Adv. Mater. 24 (35) (2012) 4756.
[236] M.K. Khaw et al., Lab Chip 16 (12) (2016) 2211.
[237] J. Seo et al., Sci. Rep. 5 (2015) 12326.
[238] J.H. Kim et al., Sci. Rep. (2015) 5.
[239] K. Seo et al., Polym. Adv. Technol. 24 (12) (2013) 1075.
[240] G. Chen et al., J. Mater. Sci. 53 (18) (2018) 13253.
[241] H. Han et al., ACS Nano 12 (2) (2018) 932.
[242] X. Tang, L. Wang, ACS Nano (2018).
[243] G. Huang et al., ACS Appl. Mater. Interfaces 9 (2) (2017) 1155.
[244] X. Gao et al., Adv. Mater. 19 (17) (2007) 2213.
[245] S. Anand et al., ACS Nano 6 (11) (2012) 10122.
[246] K. Rykaczewski et al., ACS Nano 5 (12) (2011) 9746.
[247] L. Forny et al., Powder Technol. 189 (2) (2009) 263.
[248] A. Tuteja et al., Science 318 (5856) (2007) 1618.
[249] M. Im et al., Soft Matter 6 (7) (2010) 1401.
[250] S.P. Kobaku et al., Angew. Chem. 124 (40) (2012) 10256.
[251] W. Feng et al., Adv. Mater. 28 (16) (2016) 3202.
[252] L. Sheng et al., Adv. Mater. 26 (34) (2014) 6036.
[253] J. Zhang et al., Sci. Rep. 4 (2014) 7116.
[254] I.D. Joshipura et al., ACS Appl. Mater. Interfaces 10 (51) (2018) 44686.
[255] S.S. Kadlaskar et al., J. Colloid Interface Sci. 492 (2017) 33.
[256] J. Yong et al., Adv. Mater. Interfaces 7 (6) (2020) 1901931.
[257] D. Kim et al., Sens. Actuators, B 207 (2015) 199.
[258] V. Sivan et al., Adv. Funct. Mater. 23 (2) (2013) 144.
[259] Y. Chen et al., Adv. Funct. Mater. 28 (8) (2018) 1706277.
[260] J.V. Timonen et al., Nat. Commun. (2013) 4.
[261] A. Al-Azawi et al., Small 13 (38) (2017) 1700860.

Please cite this article in press as: X. Tang et al., Materials Today, (2020), https://doi.org/10.1016/j.mattod.2020.08.013